

A Comprehensive Modeling Study of iso-Octane Oxidation

H. J. Curran ¹, P. Gaffuri, W. J. Pitz and C. K. Westbrook

Lawrence Livermore National Laboratory, Livermore, CA 94551

Abstract

A detailed chemical kinetic mechanism has been developed and used to study the oxidation of iso-octane in a jet-stirred reactor, flow reactors, shock tubes and in a motored engine. Over the series of experiments investigated, the initial pressure ranged from 1 to 45 atm, the temperature from 550 K to 1700 K, the equivalence ratio from 0.3 to 1.5, with nitrogen-argon dilution from 70% to 99%. This range of physical conditions, together with the combination of ignition delay time and species composition data, provide for a broad ranging test of the chemical kinetic mechanism. This mechanism has been developed based on our previous modeling studies of alkane combustion and, in particular, on our study of n-heptane oxidation. Experimental results of ignition behind reflected shock waves were used to develop and validate the predictive capability of reactivity of the reaction mechanism at both low and high temperatures. Moreover, species composition data from flow reactors and a jet-stirred reactor were used to help complement and refine the low and intermediate temperature portions of the reaction mechanism, leading to good predictions of intermediate product formation in most cases. In addition, a sensitivity analysis was performed for each of the combustion environments in an attempt to identify the most important reactions pertinent under the relevant conditions of study.

Corresponding Author:

Dr. Henry J. Curran

Galway-Mayo Institute of Technology,

Dublin Rd., Galway,

Ireland.

Phone: +(353)-91-742056

Fax: +(353)-91-758412

e-mail: henry.curran@gmit.ie

¹Current address: Galway-Mayo Institute of Technology, Dublin Rd., Galway, Ireland.

Introduction

There is continued interest in developing a better understanding of the oxidation of large hydrocarbon fuels over a wide range of operating conditions. Currently, there is a lot of interest in using iso-octane as a fuel in investigations of homogeneous charge compression ignition engines (HCCI), in which iso-octane is used both as a neat fuel and as a component in a primary reference fuel blend [1–4]. This interest is motivated by the need to improve the efficiency and performance of currently operating combustors and reduce the production of pollutant species emissions generated in the combustion process. Iso-octane is a primary reference fuel (PRF) for octane rating in spark-ignition engines, and when used in compression ignition engines, has a cetane number of approximately 15.

Previous experimental studies of iso-octane oxidation have focused on shock tubes [5–7], jet-stirred reactors [8–11], rapid compression machines [12–16], engines [17–19], flow reactors [20–22] and [23], in which a dynamic behaviour is observed. All of these systems exhibit phenomena including self ignition, cool flame, and negative temperature coefficient (NTC) behaviour. Furthermore, variation in pressure from 1 to 45 bar changes the temperature range over which the NTC region occurs.

Côme *et al.* [24, 25] have used an automatic generation mechanism package to create chemical kinetic mechanisms for n-heptane and iso-octane. Ranzi *et al.* [15] used a semi-detailed model to simulate the oxidation of PRF mixtures. This mechanism was further used to perform a wide range simulation of iso-octane oxidation [26]. Roberts *et al.* [27] developed a semi-detailed kinetic mechanism to simulate autoignition experiments in a co-operative fuels research engine. More recently, Curran *et al.* [28] used a detailed chemical kinetic mechanism to simulate the oxidation of PRF mixtures. This mechanism was also used to simulate flow reactor experiments on the lean oxidation of iso-octane in the intermediate temperature regime at elevated pressures [23]. Davis and Law [29] used a semi-detailed chemical kinetic mechanism to predict laminar flame speeds for iso-octane/air and n-heptane air flames.

In this study we include all of the reactions known to be pertinent to both low and high temperature kinetics. We show how the detailed kinetic model reproduces the measured results in each type of experiment, including the features of the NTC region. We discuss the specific classes of elementary reactions and reaction pathways relevant to the oxidation process, how we arrived at the rate constants for each class of reaction,

and indicate which reactions are the most important in consuming the fuel at both low and high temperature. In addition, a sensitivity analysis was carried out on each set of experimental results by changing the rate constants for different classes of reaction in the kinetic mechanism. The results of this analysis indicate the relative importance of each class of reaction and also the variation in contribution of these classes of reactions over the range of conditions of the experiments.

Model Formulation

Computer modeling of iso-octane oxidation was performed using the HCT (Hydrodynamics, Chemistry and Transport) program [30], which solves the coupled chemical kinetic and energy equations, and permits the use of a variety of boundary and initial conditions for reactive systems depending on the needs of the particular system being examined. The present detailed reaction mechanism was constructed based on the hierarchical nature of hydrocarbon–oxygen systems. The mechanism was built in a stepwise fashion, starting with small hydrocarbons and progressing to larger ones. Much of this work has been documented previously [31–34], and has been enhanced by our experience in simulating propane [35], neopentane [36,37], the pentane isomers [38], the hexane isomers [39,40], n-heptane [41] and primary reference fuel blends [28,40].

The current detailed mechanism incorporates both low- and high-temperature kinetic schemes. At higher temperatures, unimolecular fuel and alkyl radical species decomposition and isomerization reactions are especially important, while at low temperatures H atom abstraction from the fuel molecule and successive additions of alkyl radicals to molecular oxygen, leading to chain branching, dominate the oxidation process.

The low temperature submechanism is based on our detailed n-heptane chemical kinetic mechanism published previously [41]. In the interim, due to increased accuracy in both experimental and computational methods, the thermodynamic parameters associated with the low-temperature hydroperoxide species have been modified. The thermodynamic properties for the relevant radicals and stable parents were based on the group additivity method of Benson [42] using THERM [43,44] with updated H/C/O groups and bond dissociation groups [44]. We have updated the H/C/O and bond dissociation group values based on the recent studies of Lay and Bozzelli [45] and have modified these slightly so that the thermodynamic functions of $\dot{\text{R}} + \text{O}_2 \rightleftharpoons \text{RO}_2$ reactions agree with the experimental and calculated values of Knyazev and Slagle [46] for ethyl radical. These comparisons can be found in a paper by Curran *et al.* [47].

Classes of Reactions

The oxidation mechanism developed for iso-octane is formulated in the same way as that published previously for n-heptane [41]. The mechanism is developed in a systematic way, with each type of reaction in the oxidation process treated as a class of reaction with the appropriately assigned rate constant expression. Because of recent changes in thermodynamic data, and in an attempt to improve our treatment of some of our estimated rate expressions, some of those expressions published in our n-heptane paper have been changed. We outline these changes in the discussion below. The complete reaction mechanism for iso-octane oxidation includes 3600 elementary reactions among 860 chemical species. The mechanism is not presented here due to its length, but a complete copy can be obtained from the authors at the Livermore combustion website [48].

The major classes of elementary reactions considered in the present mechanism include the following:

1. Unimolecular fuel decomposition
2. H atom abstraction from the fuel
3. Alkyl radical decomposition
4. Alkyl radical + O₂ to produce olefin + H \dot{O}_2 directly
5. Alkyl radical isomerization
6. Abstraction reactions from Olefin by $\dot{O}H$, \dot{H} , \dot{O} , and $\dot{C}H_3$
7. Addition of radical species to olefin
8. Alkenyl radical decomposition
9. Olefin decomposition
10. Addition of alkyl radicals to O₂
11. $\dot{R} + R'\dot{O}_2 = R\dot{O} + R'\dot{O}$
12. Alkyl peroxy radical isomerization ($R\dot{O}_2 \rightleftharpoons \dot{Q}OOH$)

13. $\text{R}\dot{\text{O}}_2 + \text{H}\dot{\text{O}}_2 = \text{RO}_2\text{H} + \text{O}_2$
14. $\text{R}\dot{\text{O}}_2 + \text{H}_2\text{O}_2 = \text{RO}_2\text{H} + \text{H}\dot{\text{O}}_2$
15. $\text{R}\dot{\text{O}}_2 + \text{CH}_3\dot{\text{O}}_2 = \text{R}\dot{\text{O}} + \text{CH}_3\dot{\text{O}} + \text{O}_2$
16. $\text{R}\dot{\text{O}}_2 + \text{R}'\dot{\text{O}}_2 = \text{R}\dot{\text{O}} + \text{R}'\dot{\text{O}} + \text{O}_2$
17. $\text{RO}_2\text{H} = \text{R}\dot{\text{O}} + \dot{\text{O}}\text{H}$
18. $\text{R}\dot{\text{O}}$ decomposition
19. $\dot{\text{Q}}\text{OOH} = \text{cyclic ether} + \dot{\text{O}}\text{H}$ (cyclic ether formation *via* cyclisation of diradical)
20. $\dot{\text{Q}}\text{OOH} = \text{olefin} + \text{H}\dot{\text{O}}_2$ (radical site β to OOH group)
21. $\dot{\text{Q}}\text{OOH} = \text{olefin} + \text{carbonyl radical}$ (radical site γ to OOH group)
22. Addition of $\dot{\text{Q}}\text{OOH}$ to O_2
23. Isomerization of $\dot{\text{O}}_2\text{QOOH}$ and formation of carbonylhydroperoxide and $\dot{\text{O}}\text{H}$
24. Decomposition of carbonylhydroperoxide to form oxygenated radical species and $\dot{\text{O}}\text{H}$
25. Cyclic ether reactions with $\dot{\text{O}}\text{H}$ and $\text{H}\dot{\text{O}}_2$

The naming conventions used above are $\dot{\text{R}}$ and $\dot{\text{R}}'$ denoting alkyl radicals or structures and Q denoting C_nH_{2n} species or structures. For each of these classes of reactions we use the same reaction rate constant for analogous occurrences in different molecules. Thus, we assume that the abstraction of a tertiary H atom by reaction with $\dot{\text{O}}\text{H}$ radicals has exactly the same rate in 2-methyl butane, 2-methyl pentane, 3-methyl pentane and in iso-octane. Correspondingly, the total rate of tertiary H atom abstraction by $\dot{\text{O}}\text{H}$ in 2,3-dimethyl butane and in 2,4-dimethyl pentane is twice that in 2-methyl pentane, since the two former fuels have two such H atoms at tertiary sites. The n-heptane mechanism contains C_4 , C_5 and C_6 submechanisms. We treat all of the different reaction classes provided above in exactly the same way regardless of whether the fuel is n-butane, n-pentane, n-hexane or n-heptane. Our treatment of these reaction classes is described in the following sections.

High Temperature Mechanism

Reactions in classes 1–9 are sufficient to simulate many high temperature applications of iso-octane oxidation. We have made a number of *ad hoc* assumptions and approximations that may not be suitable for some problems involving alkene and alkyne fuels and further analysis is needed to refine details for these fuels. However, under the conditions of this study, iso-octane oxidation is relatively insensitive to these assumptions.

Reaction Type 1: Unimolecular Fuel Decomposition

These reactions produce two alkyl radicals or one alkyl radical and one hydrogen atom. Similar to our work on n-heptane, we calculate the rate constant expressions in the reverse direction, the recombination of two radical species to form the stable parent fuel with the decomposition reaction being calculated by microscopic reversibility. For recombinations of an alkyl radical and a hydrogen atom we assume a rate constant expression of $5 \times 10^{13} \text{ cm}^3 \text{ mol}^{-1} \text{ s}^{-1}$, based on half that recommended by Allara and Shaw [49] for $\dot{\text{H}} + \dot{\text{R}}$ recombination reactions.

There is very little information available on the rate of recombination reactions for C_2 alkyl radicals and larger. For the recombination of $\dot{\text{C}}\text{H}_3 + \dot{\text{C}}_7\text{H}_{15}$ radicals our high-pressure rate expressions are based on the recommendations of Tsang [50] for $\dot{\text{C}}\text{H}_3 + \text{t}\dot{\text{C}}_4\text{H}_9$ (methyl addition to a tertiary site), namely $1.63 \times 10^{13} \exp(+596 \text{ cal}/\text{RT}) \text{ cm}^3 \text{ mol}^{-1} \text{ s}^{-1}$ and half Tsang’s [51] recommendation for $\dot{\text{C}}\text{H}_3 + \text{i}\dot{\text{C}}_3\text{H}_7$ (methyl addition to an iso-propyl site) resulting in a rate constant of $6.80 \times 10^{14} \text{ T}^{-0.68} \text{ cm}^3 \text{ mol}^{-1} \text{ s}^{-1}$. For the recombination of $\text{t}\dot{\text{C}}_4\text{H}_9 + \text{i}\dot{\text{C}}_4\text{H}_9$ we used Tsang’s [50] recommendation of $3.59 \times 10^{14} \text{ T}^{-0.75} \text{ cm}^3 \text{ mol}^{-1} \text{ s}^{-1}$. Finally for the recombination of $\text{neo}\dot{\text{C}}_5\text{H}_{11} + \text{i}\dot{\text{C}}_3\text{H}_7$ we used a rate expression of $4.79 \times 10^{14} \text{ T}^{-0.75} \text{ cm}^3 \text{ mol}^{-1} \text{ s}^{-1}$, similar to the value used for $\text{t}\dot{\text{C}}_4\text{H}_9 + \text{i}\dot{\text{C}}_4\text{H}_9$ above.

All of these rate constant expressions were used as input in HCT and the high-pressure decomposition rate expressions calculated. These were then treated using a chemical activation formulation based on Quantum Rice-Ramsperger-Kassel (QRRK) theory, as described by Dean [52, 53] and rate constant expressions were produced at various pressures.

Reaction Type 2: H Atom Abstraction

At both low and high temperatures H atom abstraction takes place at primary, secondary and tertiary sites of iso-octane, which leads to the formation of four distinct iso-octyl radicals, Fig. 1.

The rate constant for abstraction is dependent on the type of hydrogen atom being abstracted, be it either a 1°, 2° or 3° hydrogen atom. It is also dependent on the local environment of the hydrogen atom i.e. ethane, propane, isobutane and neopentane all have 1° hydrogen atoms but their local environment is different and, on a per-hydrogen atom basis, 1° hydrogen atom abstraction by a particular radical species is slightly different. Therefore, we consider abstraction of a hydrogen atom from site (a) to be analogous to three quarter times the rate of abstraction from neopentane; hydrogen atom abstraction from site (b) analogous to 2° hydrogen atom abstraction from propane; hydrogen atom abstraction from site (c) analogous to 3° hydrogen atom abstraction from isobutane and hydrogen atom abstraction from site (d) analogous to 1° hydrogen atom abstraction from propane. We summarize these rate constant expressions in Table 1, and calculate the reverse rate constants from thermochemistry. Note that our estimates for hydrogen atom abstraction by $\text{CH}_3\dot{\text{O}}_2$ and $\text{R}\dot{\text{O}}_2$ radicals are equal to and 0.72 times those for abstraction by $\text{CH}_3\dot{\text{O}}_2$ radicals, respectively.

Reaction Type 3: Alkyl Radical Decomposition

We estimate the decomposition of alkyl radicals in the way described in our n-heptane paper [41]. Because alkyl radical β -scission is endothermic we calculate the rate constant in the reverse, exothermic direction i.e. the addition of an alkyl radical (or $\dot{\text{H}}$ atom) across the double bond of an alkene. In this way we avoid the additional complexity of the enthalpy of reaction, allowing the forward, β -scission rate constant to be calculated from thermochemistry.

Rate constants for the addition of radicals across a double bond depend on (1) the site of addition (terminal or internal C atom) and (2) the type of radical undergoing addition. Our rate constants for these addition reactions are based on the recommendations of Allara and Shaw [49]. Typically, the rate of addition of a $\dot{\text{H}}$ atom across a double bond has a pre-exponential \mathcal{A} -factor of $1 \times 10^{13} \text{ cm}^3 \text{ mol}^{-1} \text{ s}^{-1}$ with an activation energy of 1200 cal/mol if the $\dot{\text{H}}$ atom adds to the terminal C atom of the alkene, and 2900 cal/mol if the $\dot{\text{H}}$ atom adds to an internal C atom. The rate constant for the addition of an *alkyl* radical has a lower \mathcal{A} -factor and higher activation energy than for the addition of a H atom. For the addition of an alkyl radical, the \mathcal{A} -factor is approximately $8.5 \times 10^{10} \text{ cm}^3 \text{ mol}^{-1} \text{ s}^{-1}$ with an activation energy of approximately 7800 cal/mol if addition occurs at the terminal C atom and 10600 cal/mol if addition occurs at an internal C atom. We

assume these reactions are in their high pressure limit for the conditions considered in this study.

Reaction Type 4: Alkyl Radical + O₂ = Olefin + HO₂

This reaction type was discussed in some detail in our n-heptane paper. For reasons, described in that paper, we do not include reaction type 4 in our mechanisms for alkyl radical containing more than four carbon atoms. We have obtained good agreement between experimental and computational results for both C₅, C₆ and C₇ species using this assumption [39–41]. Further discussion is given below for reaction type 20.

Reaction Type 5: Alkyl Radical Isomerization

Our treatment of this reaction type has been described in our n-heptane paper. In summary, the rate constant depends on the type of C-H bond (1°, 2° or 3°) being broken, and the ring strain energy barrier involved. The activation energy (\mathcal{E}_a) is estimated, \mathcal{E}_a , using the expression,

$$\mathcal{E}_a = \Delta H_{\text{rxn}} + \text{ring strain} + E_{\text{abst}}$$

where ΔH_{rxn} is taken to be the enthalpy of reaction and is only included if the reaction is endothermic. The activation energy for abstraction is determined, following the analysis of Bozzelli and Pitz [54], from an Evans-Polanyi plot, E_{abst} vs ΔH_{rxn} (taken in the exothermic direction) of similar H atom abstraction reactions, $\text{RH} + \dot{\text{R}}' = \dot{\text{R}} + \text{R}'\text{H}$, leading to the following expression:

$$E_{\text{abst}} = 12.7 + (\Delta H_{\text{rxn}} \times 0.37)$$

The \mathcal{A} -factors were estimated to be similar to those determined for alkyl-peroxy radical isomerization (reaction type 12) described below. The rate constants employed for iso-octyl radical isomerizations are summarized in Table 2.

Reaction Type 6: H Atom Abstraction from Olefin

Our treatment of this reaction type is as described in our n-heptane paper. We assume that for olefins larger than C₄, each alkene can undergo hydrogen atom abstraction by $\dot{\text{H}}$, $\dot{\text{O}}$, $\dot{\text{O}}\text{H}$ and $\dot{\text{C}}\text{H}_3$ radicals. An approximate rate value is assumed for each abstracting radical, intended to provide a rate constant averaged over primary, secondary, allylic and vinylic C-H sites. As olefins get larger in carbon number, the double bond affects only a small portion of the molecule, the rest of which remains paraffinic in character. Thus, for large olefins, we expect the rate constants for H atom abstraction to look more like those for alkanes than smaller olefins. Furthermore, only one radical is assumed to be produced from each large olefin, which we

designate as an ‘alkenyl’ radical, an ‘average’ of the possible vinylic, allylic, primary and secondary radical species formed from n-heptane fuel.

We are aware that the most important H atom abstraction reactions from olefins are those from allylic sites. We are currently generating the appropriate thermodynamics for the radical species formed with the associated reactions and rate constant expressions. We hope to include this analysis in a later work.

Reaction Type 7: Addition of Radical Species to Olefin

This reaction type is discussed in our earlier n-heptane paper. The addition reactions of $\dot{\text{H}}$ and $\dot{\text{C}}\text{H}_3$ radicals to olefins are treated as type 3 (β -scission) reactions above. $\text{H}\dot{\text{O}}_2$ addition to olefins is considered later as the reverse of reaction type 20. $\text{R}\dot{\text{O}}_2$ addition to olefins is not considered.

The addition of an $\dot{\text{O}}\text{H}$ or a $\dot{\text{O}}$ radical to a large olefin results in the formation of an adduct but the adduct is not specifically included in the reaction mechanism. Instead, we have examined the likely β -scission products of the adduct and used those as products in this case.

Reaction Type 8: Alkenyl Radical Decomposition

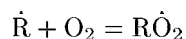
Since hydrogen atom abstraction from an olefin is greatly simplified, so too is the the subsequent consumption of the average ‘alkenyl’ radical formed to consist only of unimolecular decomposition to products we selected as being ‘reasonable’ for the fuel. The rate constants of these decompositions are all assumed to be $2.5 \times 10^{13} \exp(-45000 \text{ cal/RT}) \text{ s}^{-1}$.

Reaction Type 9: Olefin Decomposition

We have found that in model computations, the large olefin species decompose at appreciable rates. We have used, for all of these reactions, a rate constant expression of $2.5 \times 10^{16} \exp(-71000 \text{ cal/RT}) \text{ s}^{-1}$ as recommended by Edelson and Allara [55] for 1-hexene decomposition, and we have tried to select product distributions which would be expected on structural and thermochemical grounds. This is another area in which further work would improve the mechanism.

Low Temperature Mechanism

At temperatures below approximately 900 K, the predominant reactions of alkyl radicals, $\dot{\text{R}}$, is their addition to molecular oxygen,



followed by internal hydrogen atom isomerization, a second addition to O_2 , hydrogen atom isomerization and subsequent decomposition to yield two reactive hydroxyl radicals and a carbonyl radical. This sequence, as it produces three radicals from one iso-octyl radical, is responsible for the low-temperature chain-branching process. In many ways, the first addition of an alkyl radical to O_2 is the most important reaction for low temperature oxidation, even though it does not immediately determine the overall rate of chain branching.

Pollard [56] carried out an extensive kinetic analysis of hydrocarbon oxidation under low temperature conditions and identified the most important features of the low temperature submechanism. Many recent modeling studies have incorporated these features in their mechanisms. Most of these models assume that the chemical details of fuel autoignition are so complex that many simplifications are essential in order to be able to simulate the oxidation process. Some of the most prominent of these simplified model treatments of hydrocarbon ignition are the “Shell Model” [57] and related developments by Hu and Keck [58] and Cox and Cole [59]. A recent survey and critical analysis of these simplified approaches by Griffiths [60] has summarised the strengths and limitations of these models. However, our recent studies in detailed kinetic modeling of hydrocarbon oxidation [33, 37, 39, 41] have made it possible to address a wide variety of issues related to ignition, and have led to improved descriptions of ignition in internal combustion engines and engine knock.

In the following section we describe our low temperature submechanism, which includes detailed chemistry associated with the most important reactions associated with low temperature oxidation of hydrocarbon fuels as identified by earlier workers above.

Reaction Type 10: $\dot{\text{R}} + \text{O}_2$ Addition

Additions of radical species to O_2 were assumed to be dependent on the type (1° , 2° or 3°) of alkyl radical undergoing addition. For 1° and 3° alkyl radical addition we use the Lenhardt *et al.* [61] measured rates of addition for n-butyl and *tert*-butyl radicals to O_2 which are 4.52×10^{12} and $1.41 \times 10^{13} \text{ cm}^3 \text{ mol}^{-1} \text{ s}^{-1}$, respectively. Dilger *et al.* [62] measured the rate of *tert*-butyl radical addition to be $4.09 \times 10^{12} \exp(+572 \text{ cal/RT}) \text{ cm}^3 \text{ mol}^{-1} \text{ s}^{-1}$, which is a little less than half Lenhardt’s value at 700 K.

In addition, in their review, Atkinson *et al.* [63] recommend a rate expression of $6.62 \times 10^{12} \text{ cm}^3 \text{ mol}^{-1} \text{ s}^{-1}$

for $i\dot{C}_3H_7$ addition to O_2 , while Lenhardt *et al.* measured a rate expression of $1.00 \times 10^{13} \text{ cm}^3 \text{ mol}^{-1} \text{ s}^{-1}$ at 298 K. We use an “intermediate” rate expression of $7.54 \times 10^{12} \text{ cm}^3 \text{ mol}^{-1} \text{ s}^{-1}$.

The reverse decomposition rate constants are calculated from microscopic reversibility. We assume that any $C_8H_{17}\dot{O}_2$ radical, with 75 (3N-6) vibrational modes, is rapidly stabilized to its ground state, so the energy released during C-O bond formation is easily dissipated throughout the molecule. In addition, collisional stabilization is fast under the high pressure (13.5–40 bar) conditions of this study. The activation energy for the addition reaction is zero but is quite large ($\approx 30 \text{ kcal/mol}$) in the reverse, dissociation direction. Therefore, the equilibrium constant for this reaction is very strongly temperature dependent. At very low temperatures this reaction proceeds rapidly to produce the alkylperoxy species very efficiently; at high temperatures $R\dot{O}_2$ dissociates rapidly and the concentration of $R\dot{O}_2$ is very small.

In a previous neopentane oxidation study [37] a rate expression of $1.99 \times 10^{17} \text{ T}^{-2.10} \text{ cm}^3 \text{ mol}^{-1} \text{ s}^{-1}$ measured by Xi *et al.* [64] was employed for neopentyl radical addition to molecular oxygen. Furthermore, Tsang [50], in his isobutane review recommended a rate expression of $1.63 \times 10^{19} \text{ T}^{-2.70} \text{ cm}^3 \text{ mol}^{-1} \text{ s}^{-1}$ for the addition of isobutyl radicals to molecular oxygen. From these studies and the measurements of Dilger *et al.* for the addition of *tert*-butyl radicals to O_2 there appears to be a negative temperature dependence for the addition of alkyl radicals to molecular oxygen. However we do not include this dependence in our current iso-octane mechanism, but intend to add this feature to later mechanisms.

Reaction Type 11: $\dot{R} + R'\dot{O}_2 = R\dot{O} + R'\dot{O}$

Reactions of alkyl radicals with alkylperoxy radicals are estimated to occur at $7.0 \times 10^{12} \exp(+1000 \text{ cal/RT}) \text{ cm}^3 \text{ mol}^{-1} \text{ s}^{-1}$. This rate expression is based on the recommendation of Keiffer *et al.* [65] for the reaction $\dot{C}H_3 + CH_3\dot{O}_2 = CH_3\dot{O} + \dot{C}H_3O$. They recommend a rate expression of $5.06 \times 10^{12} \exp(+1411 \text{ cal/RT}) \text{ cm}^3 \text{ mol}^{-1} \text{ s}^{-1}$.

Reaction Type 12: $R\dot{O}_2$ Isomerization

Our treatment of these reactions has been adopted from Benson [66], Pollard [56], Baldwin *et al.* [67] Bozzelli and Pitz [54] and has been described in detail in our n-heptane paper [41]. Because of changes in thermodynamic parameters it has been necessary to alter our rates of isomerization. In particular, the pre-

exponential \mathcal{A} -factors have been reduced by an order of magnitude in comparison to those published in the n-heptane paper. In addition, because isomerization involves a transition-state ring, which may incorporate five, six, seven, or eight atoms, we decrease the \mathcal{A} -factor by a factor of eight as the ring size increases due to the increased change in entropy as we progressively tie up an additional rotor. This is consistent with the recommendations of Baldwin *et al.* [67] and Hughes and Pilling [68,69] in their analysis of peroxy radical isomerizations. We summarize our recommended rates of $\text{R}\dot{\text{O}}_2$ isomerization in Table 3. Using these expressions we were able to reproduce the computations for n-heptane. However, in simulating iso-octane oxidation, these expressions led to an over-prediction of the reactivity of the fuel in the temperature range 600–800 K. To reduce reactivity, all of the \mathcal{A} -factors were reduced by a factor of 0.3 from the values in Table 3. Furthermore, only the \mathcal{A} -factors involving iso-octylperoxy radicals were reduced and not those of the smaller alkyl-peroxy radicals which form part of the submechanism.

The rate expressions recommended by Baldwin *et al.* [67] and Hughes and Pilling [68,69] are qualitatively similar to those used in this paper. However, our recommendations have \mathcal{A} -factors that are approximately an order of magnitude lower and activation energies that are also lower than those recommended in the Baldwin and Pilling studies. Our modeling studies suggest that, in order to reproduce experimentally observed low to intermediate temperature alkane fuel reactivity profiles, it is necessary to use these lower activation energy values. Otherwise fuel consumption is predicted to be too slow at the start of the NTC region and too fast as the temperature increases through the NTC region.

Reaction Type 13: $\text{R}\dot{\text{O}}_2 + \text{H}\dot{\text{O}}_2 = \text{R}\text{O}_2\text{H} + \text{O}_2$

This reaction, when followed by the decomposition of $\text{R}\text{O}_2\text{H}$, converts a $\text{H}\dot{\text{O}}_2$ radical to an $\dot{\text{O}}\text{H}$ radical, which can accelerate the overall rate of reaction. However, the $\text{R}\text{O}_2\text{H}$ species is quite stable, and at sufficiently low temperature, this reaction terminates chain branching and reduces the overall rate of reaction. There is not much information available on this reaction type except for methyl and ethyl radicals. Lightfoot *et al.* [70] carried out a literature review of the reaction $\text{CH}_3\dot{\text{O}}_2 + \text{H}\dot{\text{O}}_2 = \text{CH}_3\text{O}_2\text{H} + \text{O}_2$ and recommended a rate expression of $2.47 \times 10^{11} \exp(+1570 \text{ cal}/\text{RT}) \text{ cm}^3 \text{ mol}^{-1} \text{ s}^{-1}$. Later, Atkinson *et al.* [63] also performed a literature review and recommended $2.29 \times 10^{11} \exp(+1550 \text{ cal}/\text{RT}) \text{ cm}^3 \text{ mol}^{-1} \text{ s}^{-1}$, similar to the value of Lightfoot *et al.*. In addition, Fenter *et al.* [71] measured the rate of the reaction: $\text{C}_2\text{H}_5\dot{\text{O}}_2 + \text{H}\dot{\text{O}}_2 =$

$\text{C}_2\text{H}_5\text{O}_2\text{H} + \text{O}_2$ to be $9.71 \times 10^{10} \exp(+2504 \text{ cal/RT}) \text{ cm}^3 \text{ mol}^{-1} \text{ s}^{-1}$ while Maricq and Szente [72] measured the rate to be $4.16 \times 10^{11} \exp(+1395 \text{ cal/RT}) \text{ cm}^3 \text{ mol}^{-1} \text{ s}^{-1}$.

We employ a rate expression of $1.75 \times 10^{10} \exp(+3275 \text{ cal/RT}) \text{ cm}^3 \text{ mol}^{-1} \text{ s}^{-1}$. Our rate choice is about a factor of two slower and has a stronger temperature dependence than the recommendations mentioned above. However, we expect the rate constant to decrease with increasing size of the $\dot{\text{R}}$ radical and thus our recommended rate constant.

Reaction Type 14: $\text{R}\dot{\text{O}}_2 + \text{H}_2\text{O}_2 = \text{RO}_2\text{H} + \text{H}\dot{\text{O}}_2$

We treat this reaction type in exactly the same way as described in our n-heptane paper. We have used rate constant expressions that are the same in both forward and reverse directions,

$$2.4 \times 10^{12} \exp(-10000 \text{ cal/RT}) \text{ cm}^3 \text{ mol}^{-1} \text{ s}^{-1}$$

There is little information available for this reaction rate constant except for the case where $\dot{\text{R}}$ is $\dot{\text{C}}\text{H}_3$. Our choice of rate constant is based on Tsang's recommendation [73] for $\text{CH}_3\dot{\text{O}}_2 + \text{H}_2\text{O}_2 = \text{CH}_3\text{O}_2\text{H} + \text{H}\dot{\text{O}}_2$ of $2.41 \times 10^{12} \exp(-9940 \text{ cal/RT}) \text{ cm}^3 \text{ mol}^{-1} \text{ s}^{-1}$ from 300–2500 K with an uncertainty of a factor of 5. For this isoergic reaction, the reverse rate is the same as the forward rate by analogy.

Reaction Type 15: $\text{R}\dot{\text{O}}_2 + \text{CH}_3\dot{\text{O}}_2 = \text{R}\dot{\text{O}} + \text{CH}_3\dot{\text{O}} + \text{O}_2$

The rate constants of these reactions are not particularly well known, but have been estimated as follows. Lightfoot *et al.* [74] used flash photolysis to study the reaction $\text{CH}_3\dot{\text{O}}_2 + \text{CH}_3\dot{\text{O}}_2 = \text{products}$. They reported a total rate expression of $6.02 \times 10^{10} \exp(+826 \text{ cal/RT}) \text{ cm}^3 \text{ mol}^{-1} \text{ s}^{-1}$ for the two sets of products (a) $\text{CH}_3\dot{\text{O}} + \text{CH}_3\dot{\text{O}} + \text{O}_2$ and (b) $\text{CH}_3\text{OH} + \text{CH}_2\text{O} + \text{O}_2$. In addition, they reported a ratio of $k_a/k_b = 45 \exp(-2911 \text{ cal/RT})$. We calculated the rate of reaction (b) from 300–1000 K and results fit the expression $3.11 \times 10^{14} \text{ T}^{-1.61} \exp(+1051 \text{ cal/RT}) \text{ cm}^3 \text{ mol}^{-1} \text{ s}^{-1}$. The rate expression of reaction (a) was then calculated to be $1.40 \times 10^{16} \text{ T}^{-1.61} \exp(-1860 \text{ cal/RT}) \text{ cm}^3 \text{ mol}^{-1} \text{ s}^{-1}$. The rate expression for type (a) above is the one we currently use for all type 15 reactions.

Reaction Type 16: $\text{R}\dot{\text{O}}_2 + \text{R}'\dot{\text{O}}_2 = \text{R}\dot{\text{O}} + \text{R}'\dot{\text{O}} + \text{O}_2$

This is another reaction which interconverts $\text{R}\dot{\text{O}}$ and $\text{R}\dot{\text{O}}_2$ radical species. We use the rate expression $1.40 \times 10^{16} \text{ T}^{-1.61} \exp(-1860 \text{ cal/RT}) \text{ cm}^3 \text{ mol}^{-1} \text{ s}^{-1}$ as used in the similar type 15 reaction above.

Reaction Type 17: $\text{RO}_2\text{H} = \text{R}\dot{\text{O}} + \dot{\text{O}}\text{H}$

It had been thought in the past that this reaction step was important as it produces two very reactive radical species. However, as already explained for type 13 reactions above, $\text{R}\dot{\text{O}}_2$ radical preferentially undergoes unimolecular isomerization to $\dot{\text{Q}}\text{OOH}$. Therefore, very small concentrations of stable RO_2H species are formed at low temperatures. RO_2H species can be used as sensitizers or cetane improvers and so its decomposition in those circumstances will be very important. We use a rate expression of $1.26 \times 10^{16} \exp(-42500 \text{ cal/RT}) \text{ s}^{-1}$ for this type of reaction which is approximately a factor of two faster than that recommended by Baulch *et al.* [75], and similar to the recommendations of Sahetchian *et al.* [76] for 1-heptyl and 2-heptyl hydroperoxide decomposition.

Reaction Type 18: $\text{R}\dot{\text{O}}$ Decomposition

Large alkoxy radicals undergo β -scission to generate smaller stable oxygenated species, primarily aldehydes or ketones, and a hydrogen atom or an alkyl radical species. Because alkoxy radical β -scission is endothermic we calculate the rate constant in the reverse, exothermic direction i.e. the addition of an alkyl radical (or $\dot{\text{H}}$ atom) across the double bond of an aldehyde or ketone. In this way we avoid the additional complexity of the enthalpy of reaction, allowing the forward, β -scission rate constant to be calculated from thermochemistry. The rate constant used for the reverse, addition reaction was $1.0 \times 10^{11} \exp(-11900 \text{ cal/RT}) \text{ cm}^3 \text{ mol}^{-1} \text{ s}^{-1}$.

Reaction Type 19: $\dot{\text{Q}}\text{OOH} = \text{Cyclic Ether} + \dot{\text{O}}\text{H}$

This reaction type is treated in a similar way to that published in our n-heptane paper, but has been slightly altered to be consistent with our approach of estimating \mathcal{A} -factors for $\text{R}\dot{\text{O}}_2$ radical isomerization. Taking into account loss in entropy as described earlier, we reduce the pre-exponential factor by a multiple of eight rather than twelve as one extra rotor is tied up in going from a three to four and progressively larger ring heterocycles. The rate parameters we use for these reactions are reported in Table 4.

Reaction Type 20: $\dot{\text{Q}}\text{OOH} = \text{Olefin} + \text{H}\dot{\text{O}}_2$

$\dot{\text{Q}}\text{OOH}$ species that have a radical site beta to the hydroperoxy group can decompose to yield a conjugate olefin and $\text{H}\dot{\text{O}}_2$ radical. The rate constant for this reaction was considered in the reverse direction i.e. the addition of an $\text{H}\dot{\text{O}}_2$ radical at an olefinic site, in the same way as alkyl radical decomposition (type 3 above).

The energy barrier for the addition reaction is taken from the study of Chen and Bozzelli [77] on the kinetic analysis for $\dot{\text{H}}\text{O}_2$ addition to ethylene, propene and isobutene. They recommend an activation energy for the addition of $\dot{\text{H}}\text{O}_2$ to the terminal carbon atom in the double bond of approximately 12.5 kcal/mol. For $\dot{\text{H}}\text{O}_2$ addition to the ‘internal’ carbon atom on propene they recommend an activation energy of 11 kcal/mol and for $\dot{\text{H}}\text{O}_2$ addition to the ‘internal’ carbon atom on isobutene an activation energy of 7.6 kcal/mol is recommended. All values are in the high-pressure limit. Thus, following Chen and Bozzelli we use the activation energies recommended above by them depending on the type of carbon atom the $\dot{\text{H}}\text{O}_2$ radical bonds to. A pre-exponential \mathcal{A} -factor of 1.0×10^{11} is typically used. It is worth noting that the activation energy for this class of reaction *decreases* with the type (1° , 2° or 3°) olefinic carbon atom to which the $\dot{\text{H}}\text{O}_2$ radical is bonding. However, for type 3 reactions above the activation energy *increases* with the type of olefinic carbon atom.

Recent studies have shown that, for the case of ethyl radical adding to O_2 , the reaction does not proceed through the $\dot{\text{Q}}\text{OOH}$ path to olefin plus $\dot{\text{H}}\text{O}_2$ radical, but reacts through a $\dot{\text{H}}\text{O}_2$ radical elimination channel [78]. It is reasonable to expect that other larger alkyl radicals react with O_2 and proceed through a $\dot{\text{H}}\text{O}_2$ radical elimination channel as well. We have not, as yet, included this new information in our reaction mechanism. If this molecular elimination channel is the important channel for all alkyl radicals then the $\dot{\text{Q}}\text{OOH} = \text{olefin} + \dot{\text{H}}\text{O}_2$ reaction will be replaced in our mechanism by an $\text{alkyl} + \text{O}_2 = \text{olefin} + \dot{\text{H}}\text{O}_2$ reaction whose rate is determined by the rate of $\dot{\text{H}}\text{O}_2$ radical elimination from the excited state alkylperoxy radical adduct.

Reaction Type 21: $\dot{\text{Q}}\text{OOH} = \text{Olefin} + \text{Carbonyl Radical}$

$\dot{\text{Q}}\text{OOH}$ species, produced by an $\text{R}\dot{\text{O}}_2$ isomerization with an intermediate ring structure of six atoms can undergo β -scission. We treat this class of reaction in exactly the same way as an alkyl radical (type 3), alkoxy radical (type 18) or $\dot{\text{Q}}\text{OOH} = \text{olefin} + \dot{\text{H}}\text{O}_2$ (type 20) β -scission. The reverse addition of the carbonyl radical to the olefin is estimated to be $1.00 \times 10^{11} \exp(-11900 \text{ cal/RT}) \text{ cm}^3 \text{ mol}^{-1} \text{ s}^{-1}$ with the forward rate expression calculated from thermochemistry.

Reaction Type 22: Addition of $\dot{\text{Q}}\text{OOH}$ to O_2

The rate expressions for this class of reaction are identical to those for alkyl addition to O_2 , type 10. The

reverse dissociation rate was then calculated from microscopic reversibility.

Reaction Type 23: $\dot{\text{O}}_2\text{QOOH}$ Isomerization to Carbonylhydroperoxide + $\dot{\text{O}}\text{H}$

The rate constant for this and other isomerizations *via* an internal hydrogen atom transfer are analogous to those for $\text{R}\dot{\text{O}}_2 \rightleftharpoons \dot{\text{Q}}\text{OOH}$ isomerization. Similar to our n-heptane work, the activation energy has been reduced by 3 kcal mol⁻¹ as the hydrogen atom being abstracted is bound to a carbon atom which is bound to a hydroperoxy group and should be more easily removed. In addition, the \mathcal{A} -factors have been reduced by a factor of three consistent with our treatment of alkyl-peroxy radical isomerization, reaction type 12.

Reaction Type 24: Carbonylhydroperoxide Decomposition

The decomposition of carbonylhydroperoxide molecules leads to the formation of two radicals, a carbonyl radical and a second $\dot{\text{O}}\text{H}$ radical, which results in chain branching as two radical species are produced from one stable reactant.

A rate expression of $1.5 \times 10^{16} \exp(-42000 \text{ cal}/RT) \text{ s}^{-1}$ was chosen for the decomposition of each carbonylhydroperoxide molecule even though each species has slightly different thermodynamic properties. Our rate constant expression is similar to that used for alkylhydroperoxide decomposition based largely on the recommendations of Sahetchian *et al.* [76] for 1-heptyl and 2-heptyl hydroperoxide decomposition. Carbonylhydroperoxide decomposition is especially important at low temperatures as the high activation energy ensures an induction period during which carbonylhydroperoxide concentration builds up. The subsequent decomposition products help accelerate the overall rate of fuel oxidation, raising the temperature and allowing the remaining carbonylhydroperoxide species to decompose more easily.

Reaction Type 25: Cyclic Ether Reactions with $\dot{\text{O}}\text{H}$ and $\text{H}\dot{\text{O}}_2$

Cyclic ethers are produced under low temperature conditions during hydrocarbon oxidation and, in the present study are large C₈ species with an oxygen atom embedded in the molecule. Therefore, it is reasonable to assume that the reaction proceeds by means of hydrogen atom abstraction. As the two most prevalent radicals are $\dot{\text{O}}\text{H}$ and $\text{H}\dot{\text{O}}_2$ at low and intermediate temperatures, where the cyclic ethers are produced, these are the only two radical attack reactions included. The rate expressions used are published in our n-heptane paper [41]. In addition, hydrogen atom abstractions can be easily extended to include abstractions by $\dot{\text{H}}$,

$\dot{\text{C}}\text{H}_3$ and $\dot{\text{O}}$ radicals, for example. However, we have not included these reactions in the current study.

Reaction Mechanism

The overall reaction scheme included in this study for iso-octane oxidation is depicted in Fig. 2. The naming conventions used are $\dot{\text{R}}$ and $\dot{\text{R}}'$, denoting alkyl radicals; in $x\dot{\text{C}}_8\text{H}_{16}\text{OOH} - y$, x denotes the site of the hydroperoxyl group and y the radical site for two of the four distinct sites on the iso-octane molecule shown in Fig. 1, and $i\text{C}_8\text{ket}$ refers to iso-octyl carbonylhydroperoxide species.

At high temperatures, the overall reaction pathway proceeds *via* β -scission of the alkyl radicals $\dot{\text{R}}$ proceeding rapidly to a smaller olefin and other species, with chain branching due primarily to the reaction $\dot{\text{H}} + \text{O}_2 = \dot{\text{O}} + \dot{\text{O}}\text{H}$. At low temperatures, chain branching is mainly due to the reaction pathway leading through the carbonylhydroperoxide species. As the temperature increases, the chain propagation reactions of $\dot{\text{Q}}\text{OOH}$ species increase, because the energy barrier to their formation is more easily overcome, leading to the formation of cyclic ether species, conjugate olefins, and β -decomposition products, at the expense of the reaction pathways through the carbonylhydroperoxide species. The increasing importance of these propagation channels leads to a lower reactivity of the system which is observed as the NTC region. The difference in the chain branching mechanisms at low and high temperatures leads to varying reactivity depending on the fuel to air equivalence ratio. Because the chain branching mechanism at high temperatures is due to the $\dot{\text{H}} + \text{O}_2 = \dot{\text{O}} + \dot{\text{O}}\text{H}$ reaction, fuel lean mixtures are more reactive in this regime. However, at low temperatures, because chain branching is dependent on radical species formed directly from the parent fuel, fuel rich mixtures are oxidized more quickly.

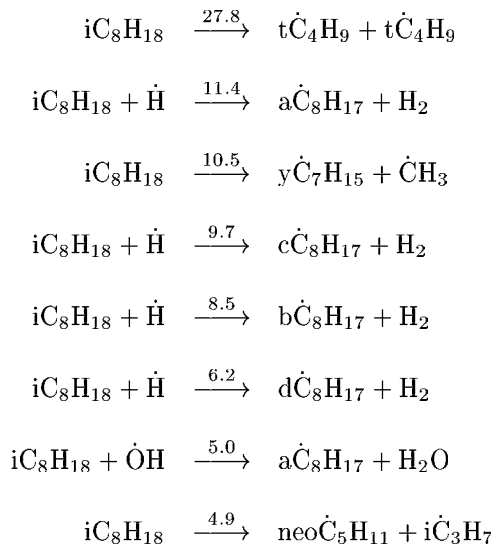
Mechanism Validation

An explanation of the chemical kinetic mechanism formulation has been given in the preceding section. Below, we describe how this mechanism was used to simulate experimental results obtained in an atmospheric pressure flow reactor [20], a variable pressure flow reactor [15,22] at 12.5 atm, and a complementarily different flow reactor [23]. Moreover, results obtained in a jet-stirred reactor [10], shock tubes [5–7] and in a motored engine [17] are also simulated. Overall, good agreement is obtained between model and experiment. We indicate the major pathways responsible for fuel oxidation under the specific conditions of each study and also point out where we believe improvements may be made.

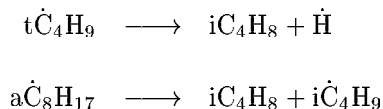
Atmospheric Pressure Flow Reactor

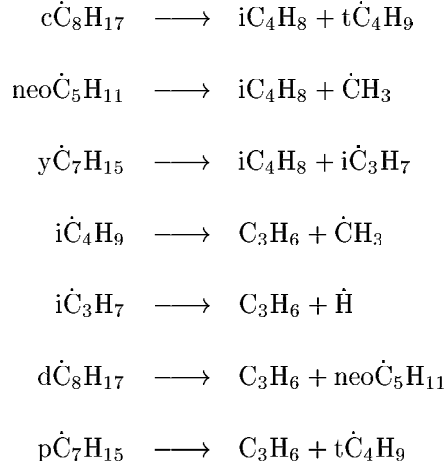
Experiments, carried out in an adiabatic flow reactor, provide a well-characterized environment that is designed to minimize mixing and diffusion effects. Dryer and Brezinsky [20] studied the oxidation of iso-octane in an atmospheric-pressure flow reactor at 1080 K, and at an equivalence ratio of one. It was found that the oxidation of iso-octane produced primarily iso-butene (iC_4H_8) and propene (C_3H_6) as intermediate products. In addition, methane (CH_4), ethane (C_2H_6), ethylene (C_2H_4), 2-methyl-1-butene (aC_5H_{10}), allene (C_3H_4 -a), carbon monoxide (CO) and carbon dioxide (CO_2) were also quantified. Simulations were performed under the assumption of plug flow: the velocity and temperature profile in the reactor is radially uniform and axial diffusion of species and energy is negligible. Constant pressure and adiabatic walls were also assumed. The experimental results together with the model predictions are depicted in Fig. 3.

Analysis of HCT output reveals that, at 50% fuel consumption, unimolecular decomposition and hydrogen atom abstraction from the fuel by hydrogen atoms predominates the consumption of the fuel. The reactions are, in order of contribution:



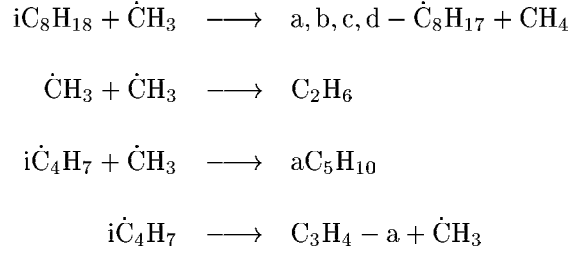
The values over the arrows give the importance, on a scale of 0–100, of each reaction to the consumption of iso-octane at 50% consumption. Isobutene and propene are the major intermediates produced under these conditions and it is apparent, from the equation arrays above and below, why this is so.





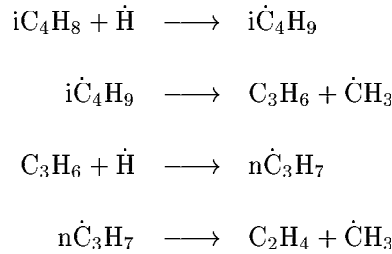
($\text{y}\dot{\text{C}}_7\text{H}_{15}$ = 2,4-dimethyl-propan-2-yl radical and $\text{p}\dot{\text{C}}_7\text{H}_{15}$ = 2,2-dimethyl-propan-2-yl radical).

Methane is produced via hydrogen atom abstraction from the fuel by methyl radicals, and ethane by the recombination of methyl radicals. 2-methyl-1-butene is produced by the reaction of methyl radicals with 2-methyl-allyl radicals. The decomposition of 2-methyl-allyl radicals produces allene and a methyl radical.



The experimental carbon monoxide profile is not well reproduced by the model, Fig. 3a. It appears from the experimental result that there is a direct path forming CO while the model predicts that CO is mainly formed from formaldehyde oxidation via formyl radical consumption i.e. secondary processes.

The concentration of ethylene and methane are also underpredicted by the model. We believe that there may be a mechanism that we are not fully reproducing correctly in the model. Namely, we believe that there is a sequence of reactions of isobutene and propene as follows:



Of course, addition of a hydrogen to isobutene and propene also lead to the production of tert-butyl and isopropyl radical, respectively. However, the above sequence converts isobutene and a hydrogen atom into propene and an methyl radical and similarly, propene and a hydrogen atom into ethylene and a methyl radical. Our chemical kinetic model does contain all of these reactions but may not be accurately represented. Certainly, increasing the importance of this sequence of reactions would make our predictions of methane and ethylene more consistent with those measured experimentally.

Princeton Variable Pressure Flow Reactor

Iso-octane was studied under very high dilution (99% N₂), the initial concentration of fuel being 0.14%, at $\phi = 1.0$ in the temperature range 600–850 K and at a constant pressure of 12.5 atm [15, 22]. Data were obtained for the mole fractions of CO, CO₂, H₂O, O₂, and the temperature at the fixed sampling locations. These data together with the model simulations are depicted in Fig 4.

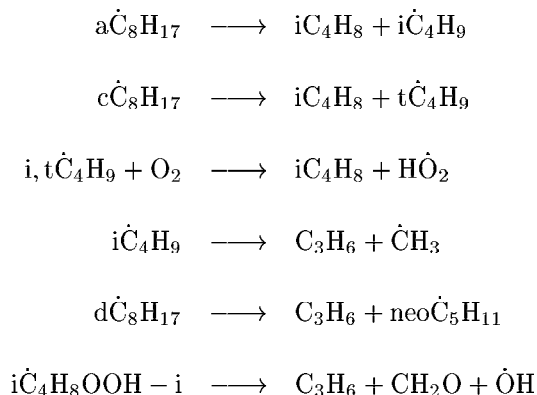
It is clear that, in the temperature range 600–675 K, the model simulation predicts more reactivity than observed experimentally, with more O₂ reacted and more CO, CO₂, and H₂O produced. We have not been able to gain better agreement as to do so would result in poorer agreement with the shock tube ignition-delay data of Fieweger *et al.* [6, 7], discussed below.

Lean Oxidation in a Variable Pressure Flow Reactor

Complementary to the experiments performed above under stoichiometric conditions, Chen *et al.* [23] investigated iso-octane in a high pressure flow reactor at a temperature of approximately 925 K, at 3, 6 and 9 atm pressure and with a fuel/air equivalence ratio of approximately 0.05, in which the mole fractions of iso-octane, oxygen, and nitrogen were 0.08%, 20.99%, and 78.92%, respectively. Many hydrocarbon and oxygenated hydrocarbon intermediates were identified and quantified as a function of time. These experimental results provide a stringent test of the low temperature chemistry portion of the kinetic model as they emphasise the importance of alkyl radical addition to molecular oxygen and internal H-atom isomerization reactions relative to alkyl radical decomposition reactions. Comparisons of model predictions with many experimentally measured species at 6 atm and 945 K are depicted in Figs. 5 and 6.

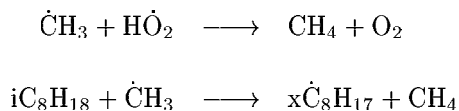
Overall, there is good agreement between model and experiment, and so it is reasonable to assume that the mechanism is predicting the major production routes correctly. Olefins are the main products formed in

the oxidation process, of which isobutene (iC_4H_8) is formed in highest concentrations followed by propene (C_3H_6), Fig. 5b. Below, we list the reactions responsible for isobutene and propene formation in order of decreasing importance.

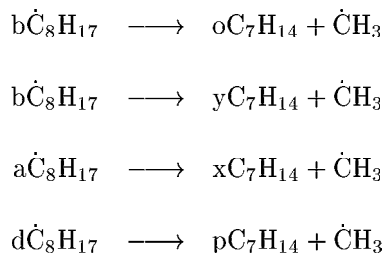


In $i\dot{C}_4H_8OOH-i$ the hydroperoxyl group is attached to one of the substituted methyl groups while there is a radical site on one of the other two methyl groups.

Methane (CH_4) is generated by the reaction of methyl radicals with hydroperoxyl radical and with the fuel, Figs 5b.

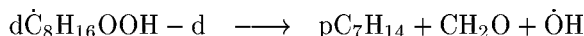
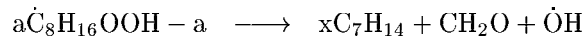
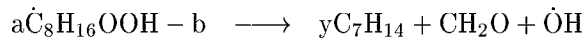
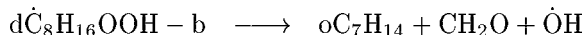


Significant quantities of the C_7 olefins are formed including 4,4-dimethyl-pent-2-ene (oC_7H_{14}), 2,4-dimethyl-pent-2-ene, (yC_7H_{14}), 2,4-dimethyl-pent-1-ene (xC_7H_{14}) and 4,4-dimethyl-pent-1-ene (pC_7H_{14}), Fig. 5c.



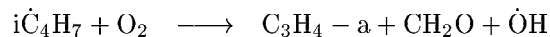
The model indicates that the C_7 olefins are formed almost exclusively by β -scission of iso-octyl radicals under the conditions of this study. Note that the decomposition of 2,4,4-trimethyl-pent-3-yl radical, ($b\dot{C}_8H_{17}$), leads to the formation of almost equal quantities of 2,4- and 4,4-dimethyl-pent-2-ene. C_7 olefins

can also be formed through low temperature reaction paths. The model indicates that very small amounts ($\approx 5\%$) are generated from octyl-hydroperoxide radical β -scission.

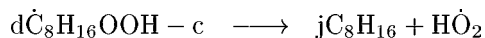


In $d\dot{C}_8H_{16}OOH - b$, 'd' refers to the site at which the hydroperoxyl group is attached and 'b' to the radical site on iso-octane.

There are various other hydrocarbon species produced, including allene (C_3H_4 -a), ethylene (C_2H_4), ethane (C_2H_6), 2,4,4-trimethyl-pent-1-ene (jC_8H_{16}), and 2-methyl-1-butene, (aC_5H_{10}), Fig. 5d. Allene is formed in appreciable concentrations and is predicted to be generated from the reaction of 2-methyl-allyl radical with molecular oxygen *via* the overall reaction:



Small concentrations of 2,4,4-trimethyl-pent-1-ene (jC_8H_{16}) were measured and this olefin is predicted to be formed from the β -scission of a hydroperoxy-octyl radical:



2-methyl-1-butene (aC_5H_{10}) is predicted to be formed by the reaction of 2-methyl-allyl with methyl radicals, although it is very much underpredicted by the model indicating that there may be an alternative route to its formation. (Note that in the atmospheric-pressure experiments of Dryer and Brezinsky [20] 2-methyl-1-butene is slightly over-predicted.)

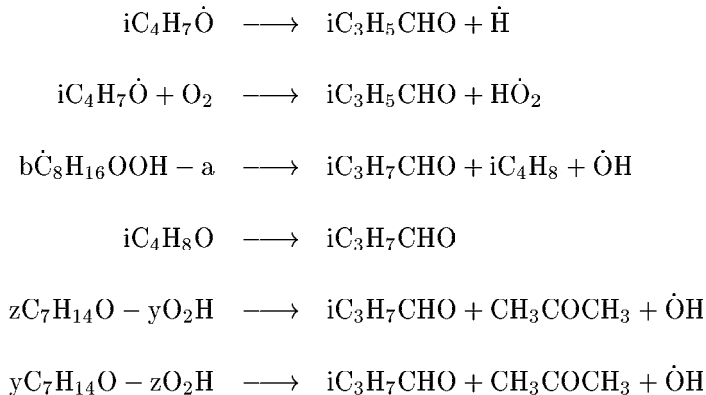


In Fig. 5c the lowest solid line corresponds to the model predicted 2-methyl-but-1-ene concentrations.

Of the oxygenates, acetone (CH_3COCH_3), methacrolein (iC_3H_5CHO) and isobuteraldehyde (iC_3H_7CHO) are formed in relatively high concentrations, Fig. 6a. Acetone, although underpredicted by just less than a

factor of two, is predicted to be formed through the Waddington mechanism [79, 80] mainly from isobutene, Fig. 7 with a small quantity formed from the C₇ olefins at high fuel conversion.

2-methyl-allyl radicals can react with hydroperoxyl radicals creating methallyl-oxyl radicals which decompose to yield methacrolein and a hydrogen atom. As these experiments were performed under very lean conditions some methallyl-oxyl radicals also react with molecular oxygen to produce methacrolein and hydroperoxyl radicals.



Isobuteraldehyde is mainly produced from the β -scission of 2,4,4-trimethyl-3-hydroperoxy-pent-1-yl radical ($\text{b}\dot{\text{C}}_8\text{H}_{16}\text{OOH}-\text{a}$) and also from the isomerization of isobutene oxide [81]. At higher fuel conversion some isobuteraldehyde (and acetone) is also produced from 2,4-dimethyl-pent-2-ene *via* the Waddington mechanism.

Relatively low concentrations of cyclic ethers were measured including 2,2,4,4-tetramethyl-tetrahydrofuran (TMTHF, iC_8eterac), isobutene oxide ($\text{iC}_4\text{H}_8\text{O}$), 2-isopropyl-3,3-dimethyl oxetane (iC_8eterab) and 2-tert-butyl-3-methyl oxetane (iC_8eterbd), Fig. 6b. In this figure the lower dotted line corresponds to iC_8eterbd .

The C₈ cyclic ether species are predicted to be formed from the corresponding hydroperoxy-octyl radical, see for example Fig. 8.

It is evident from Fig. 6b that all of the C₈ cyclic ethers are grossly underpredicted by the kinetic model. It appears that the above mechanism cannot account for their formation. In contrast, isobutene oxide is well predicted by the model. It is formed by the direct reaction of isobutene with a $\text{H}\dot{\text{O}}_2$ radical as recommended

by Baldwin *et al.* [82]:



We use the rate expression of Baldwin *et al.* of $1.29 \times 10^{12} \exp(-13340 \text{ cal/RT}) \text{ cm}^3 \text{ mol}^{-1} \text{ s}^{-1}$ for this reaction. Obviously, we need to improve our treatment of olefin plus hydroperoxyl radical addition reactions. In particular, it seems appropriate to include some chemically activated pathways, consistent with that postulated by Baldwin and co-workers for isobutene plus hydroperoxyl radical above.

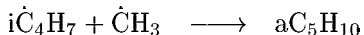
Jet Stirred Reactor

Dagaut *et al.* [10] investigated iso-octane oxidation in a jet-stirred reactor at 10 atm, in the temperature range 550–1150 K, with equivalence ratios of 0.3, 0.5, 1.0 and 1.5, and 99% dilution by nitrogen with a residence time of 1 s. Simulations were performed under isothermal, constant pressure conditions, and assumed perfect mixing of the reactants. Time dependent calculations were run for long times until a steady state solution was obtained. Reactant concentrations and intermediate and final product concentrations were quantified and the results, together with the mechanism simulations, are depicted in Figs. 9–11.

Fig. 9 shows comparisons between computed and experimental results for stoichiometric mixtures of 0.1% iso-octane. Overall, species concentrations are reproduced quite well by the model. Fig. 9a shows the profiles for the fuel, carbon monoxide and carbon dioxide. All profiles are well simulated by the model. Fig. 9b depicts profiles for methane, isobutene, ethylene and propene. Methane and ethylene peak at 975 K, while isobutene and propene peak at 850 K. In addition, all of the C₇ olefins peak at 850 K, Fig. 9c and d. The products formed at lower temperature appear as ‘primary’ products of the oxidation process while those that peak at higher temperature are produced as ‘secondary’ products. At 820 K, under stoichiometric conditions where 60% of the fuel has been oxidised, iso-octane undergoes hydrogen atom abstraction, primarily by hydroxyl radicals but also by hydrogen atoms and hydroperoxyl radicals, producing the four iso-octyl radicals. These radicals decompose to produce isobutene, propene and the C₇ olefins as illustrated in the equation arrays earlier during the discussion of iso-octane oxidation in a flow reactor.

The production of methane and ethane at 950 K is a consequence of the formation of methyl radicals which can recombine or abstract a hydrogen atom from another species. In Fig. 9d the higher concentration solid line corresponds with the over-prediction of 2,4-dimethyl-1-pentene (xC₇H₁₄) while the lower solid line is the

simulated underprediction of 2-methyl-1-butene (aC_5H_{10}). Moreover, our model overpredicts the formation of 2-methyl-1-butene in the atmospheric flow reactor experiments but also underpredicts its formation in lean oxidation flow reactor experiments at 6 atm. We believe that 2-methyl-1-butene is generated from the recombination of methyl and 2-methyl-allyl radicals.



A pressure dependent treatment of this reaction is needed in order to improve the mechanism’s capability of simulating 2-methyl-1-butene formation.

Variations in equivalence ratio at constant pressure were found to change the overall reactivity of this system. Under fuel-lean conditions, Fig. 10, the fuel is oxidised at lower temperature relative to stoichiometric conditions, while, under fuel-rich conditions, oxidation occurs at higher temperatures relative to the stoichiometric experiments, Fig. 11. This behaviour is well reproduced by the simulation. In addition, under fuel-lean conditions, lower concentrations of hydrocarbon intermediates are produced, while under fuel-rich conditions higher concentrations are produced relative to the stoichiometric condition.

Shock Tube

Our detailed chemical kinetic model has been used, assuming constant-volume, homogeneous, adiabatic conditions behind the reflected shock wave, to simulate the autoignition of iso-octane, at high temperatures studied by Vermeer *et al.* [5] and at low temperatures as studied by Fieweger *et al.* [6,7]. Vermeer *et al.* studied the autoignition of iso-octane/oxygen/argon mixtures behind reflected shock waves in the pressure range of 1-4 atm and the temperature range of 1200–1700 K. Stoichiometric fuel-oxygen mixtures were diluted with 70% argon in order to reduce the influence of the boundary layer. We have obtained good agreement between experiment and simulation as observed in Fig. 12. It should be noted that in our n-heptane study [41] we also simulated data for n-heptane under almost identical conditions. However, the simulation was substantially faster than the experimentally measured delay times. We speculated that this may have been due to our estimation of the unimolecular decomposition of the fuel being in the high pressure limit and that we should include a pressure-dependent treatment of this type of reaction to improve our predictions. In our description of unimolecular decomposition (reaction type 1) we have included a pressure-dependent treatment and we have obtained good agreement with the experimental results.

Fieweger *et al.* studied the ignition of iso-octane/air mixtures behind both incident and reflected shock waves at equivalence ratios of 0.5, 1.0 and 2.0 in the temperature range 700–1300 K at reflected-shock pressures from 13–45 bar, conditions similar to those in an operating engine. Overall, good agreement is observed between the model and the experimental results, Figs. 13–15. However, at temperatures below about 800 K the model is consistently slower than the experimental measurement. Fig. 13 depicts ignition delay times versus inverse temperature for the stoichiometric oxidation of iso-octane in air at 13 bar in the temperature range 950–1300 K. The computed results very clearly depict a very fundamental feature of fuel oxidation kinetics. Namely, that under these conditions at temperatures below approximately 1150 K, fuel-rich mixture ignite faster than fuel lean mixtures. At 1150 K all mixtures ignite at approximately the same time and at temperatures above 1150 K fuel lean mixtures ignite faster than fuel rich mixtures. This is due to the nature of the chain-branching process. At high temperature it is due to the reaction of hydrogen atom with molecular oxygen to produce a hydroxyl radical and an oxygen atom. At low temperatures, the production of carbonyl-hydroperoxide species, which lead to chain branching, is directly proportional to the fuel concentration.

Fig. 14 shows comparisons of model predicted and experimentally measured ignition delay times versus inverse temperature at a reflected shock pressure of 40 bar for lean, stoichiometric and rich mixtures. In the temperature range 770–910 K, both model and experiment depict an obvious negative temperature coefficient (NTC) behaviour, in which the ignition delay time becomes longer as the temperature increases.

Finally, Fig. 15 shows the influence of pressure on ignition delay for stoichiometric fuel in air mixtures. As the pressure is increased the ignition delay times become shorter. In addition, at reflected shock pressures of 34 bar and higher it is possible to measure ignition delays to a temperature of 700 K and thus observe an NTC behaviour. There is good agreement between model and experiment in all instances, even though the mechanism consistently overpredicts the ignition delay time at low temperatures.

Co-Operative Fuels Research Engine

Leppard [17] performed autoignition experiments in a CFR engine motored at 500 RPM using n-heptane, iso-octane and PRF mixtures, and speciated the exhaust gases. At an intake manifold pressure of 120 kPa and temperature of 448 K, Leppard started sampling the exhaust gas at a compression ratio (CR) of 6.0.

The compression ratio was increased in steps of 0.5, with continuous sampling, until iso-octane autoignited. Fig. 16 depicts the experimentally measured profiles for carbon monoxide and molecular oxygen (points) are plotted together with the model predictions (lines). Iso-octane is observed to autoignite at a critical compression ratio (CCR) of 10.7, while at a CR of 10.5 autoignition is not observed although 36% of the fuel had reacted. Thus, autoignition occurs at any CR higher than 10.7, i.e. to the right of the straight dashed line in Fig. 16. The model predicts a CCR of between 10.5 and 10.75 with 61.6% of the fuel oxidised at a compression ratio of 10.5. Moreover, even though the CCR for iso-octane is well reproduced by the model, it is apparent that, because the concentration of carbon monoxide formed is a direct measure of reactivity, at all compression ratios the model predicts more reactivity than is observed experimentally.

The prediction of intermediate speciation data measured in engine experiments is extremely difficult, as the system passes through a wide range of temperature and pressure within the engine, and the exhaust flow which is analyzed here is also unsteady. We believe that overall, good agreement is observed between model prediction and experimental observation, although some refinements may be possible in the chemistry. Table 6 shows experimentally quantified species concentrations together with those predicted by the detailed mechanism, both at 36% fuel conversion. Isobutene was the largest measured alkene component by a factor of five, with propene, di- and tri-methyl pentenes composing the remainder. The model predicts isobutene formation in greatest abundance, but is overpredicted by a factor of two, while propene is overpredicted by less than a factor of two. Of the olefins, the predicted concentrations of 2,4-dimethyl-2-pentene, 2,4,4-trimethyl-1-pentene and 2,4,4-trimethyl-2-pentene are quite good even though the relative concentrations of the tri-methyl pentenes are reversed. In addition, 4,4-dimethyl-2-pentene is underpredicted by about an order of magnitude.

The only alkanes identified were methane (in trace amounts) and iso-octane. Of the measured oxygenates, formaldehyde, 2,2,4,4-tetramethyl-tetrahydro-furan (TMTHF) and acetone were present in the greatest amounts, followed by 2-tert-butyl-3-methyl oxetane, 2-isopropyl-3,3-dimethyl oxetane, isobuteraldehyde and methacrolein. Both formaldehyde and acetone are overpredicted by more than a factor of two. TMTHF is underpredicted by less than a factor of three and the oxetanes are also underpredicted by almost an order of magnitude. Isobuteraldehyde and methacrolein are reasonably well predicted by the model.

Li et al. [19] studied iso-octane autoignition in a motored, single-cylinder engine and obtained in-cylinder samples at different points prior to autoignition. They found that isobutene and TMTHF were the major intermediates formed during iso-octane oxidation in agreement with Leppard’s experiments. In addition, the di- and tri-methyl pentenes were also observed, as were the C₁ to C₄ aldehydes and C₈ oxetane species. 2,2-dimethyl propanal was also detected in trace amounts.

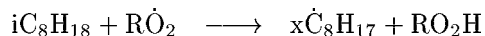
Sensitivity Analysis

A detailed analysis was carried out to investigate the sensitivity of each class of reaction denoted earlier, to the oxidation of iso-octane in each experiment. Sensitivity analyses were performed by multiplying the rate constants of a particular class of reaction by a factor of two (both forward and reverse rates) and then calculating the percent change in reactivity. In the case of the shock tube experiments of Fieweger *et al.* [6,7] for example, we calculated the percent change in ignition delay time compared with the baseline simulation. A positive percent change indicates a longer ignition delay and a decreased overall reaction rate, and a negative change indicates an increased overall reactivity of the system. Three different temperatures were chosen to help indicate sensitivity of each class to the onset, middle and end of the NTC region at an average pressure of 40 bar. The reaction rate constants that exhibited the highest sensitivity are shown in Fig. 17. Reactions in which we multiplied both forward and reverse rate constants by a factor of two are denoted with an equal to “=” sign between reactants and products and reactions in which we multiplied only the forward rate constant (i.e. effected a change in the equilibrium constant) are denoted with an arrow “⇒” between reactants and products. In addition, for the low temperature shock tube experiments of Fieweger *et al.* our analysis has mainly focused on the classes of reaction which are represented in Fig. 2. We did include sensitivity to reactions such as $\dot{\text{O}}\text{H} + \dot{\text{O}}\text{H} + \text{M} = \text{H}_2\text{O}_2 + \text{M}$. We have used the chemistry edits from the HCT code to identify the important reactions occurring under these conditions. However, because we performed a brute-force analysis we cannot be certain that we have identified all of the sensitive reactions.

In order to understand the sensitivity analysis pertaining to the shock tube results of Fieweger *et al.* it is appropriate to refer to Fig. 2. In particular, at the relatively low temperatures of this study the fate of the $\dot{\text{Q}}\text{OOH}$ species is all important. Reactions which promote the route leading to $\dot{\text{Q}}\text{OOH}$ formation and its subsequent route to chain branching via its addition to molecular oxygen result in a negative sensitivity

coefficient (increased reactivity), while reactions which lead to the decomposition of the $\dot{Q}OOH$ radical show a positive sensitivity coefficient (decreased reactivity).

The reaction with the highest negative sensitivity, and thus increases the rate of oxidation is the reaction of the fuel with alkyl-peroxy radicals:

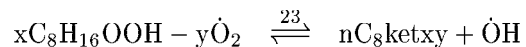


This sensitivity was not observed in our studies of n-heptane oxidation. However, we have reduced our rate expressions for $R\dot{O}_2 \rightleftharpoons \dot{Q}OOH$ isomerization reactions and this has led to an increased importance of the bimolecular reaction above. The negative sensitivity to this reaction is understandable because this reaction leads to the formation of alkyl radicals in addition to stable alkylhydroperoxide species which can decompose to form an alkoxy- and a hydroxyl radical.

$R\dot{O}_2 \rightleftharpoons \dot{Q}OOH$ isomerization reactions also show a strong negative sensitivity coefficient. Indeed, either increasing the rate expression by a factor of two, with or without a change in equilibrium constant, leads to almost identical negative sensitivity coefficients at all temperatures.

Another reaction type that increases the overall reactivity of the system is the addition of alkyl radicals to molecular oxygen, reaction type 10. Interestingly, increasing the rate expressions by a factor of two without affecting the equilibrium constants has very little effect. However, a change of a factor of two in the equilibrium constant shows a high negative sensitivity coefficient. This result indicates that our simulations are predicting the $\dot{R} + O_2 \rightleftharpoons R\dot{O}_2$ to be in equilibrium at all reflected shock temperatures and that the thermodynamic parameters used for the alkyl and alkylperoxy radicals are very important. This behaviour is also observed for the addition of hydroperoxy alkyl radicals to molecular oxygen, reaction type 22. A change in equilibrium constant leads to an increase in reactivity, while a change in overall rate has very little effect on the reactivity of the system.

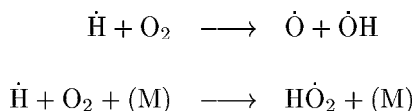
The isomerization of the peroxy-alkylhydroperoxide radical to form a carbonyl-hydroperoxide molecule and $\dot{O}H$ radical, reaction type 23, also shows a high negative sensitivity.



In $x\text{C}_8\text{H}_{16}\text{OOH} - y\dot{\text{O}}_2$, x refers to the carbon atom to which the OOH group is attached and y refers to the site where the O_2 group is attached. In $n\text{C}_8\text{ketxy}$, x refers to the carbon with the carbonyl group attached and y refers to the site where the hydroperoxy group is attached. We have also observed identical sensitivity to changing the equilibrium constant of this reaction by a factor of two i.e. multiplying the forward rate by two but maintaining the reverse rate at its usual value. This result is expected, as the reverse rate of addition of $\dot{\text{O}}\text{H}$ radical to the carbonylhydroperoxide is very slow and is not observed computationally.

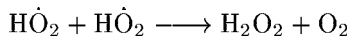
In addition, we observe high negative sensitivity coefficients to hydrogen atom abstraction reactions from the fuel by $\text{H}\dot{\text{O}}_2$, $\text{CH}_3\dot{\text{O}}_2$ and $\dot{\text{O}}\text{H}$ radicals. In particular, the importance of the abstractions by $\text{H}\dot{\text{O}}_2$ and $\text{CH}_3\dot{\text{O}}_2$ radicals becomes more pronounced at higher temperatures. This is a reflection of the importance of intermediate temperature kinetics in the range 825–1000 K.

Hydroperoxyl radical chemistry and $\text{H} + \text{O}_2 = \dot{\text{O}} + \dot{\text{O}}\text{H}$ chain branching reactions are also important.



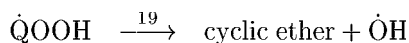
In the above sequence the reaction producing oxygen atoms and hydroxyl radicals is chain branching and thus promotes reactivity while the second, competing reaction, reduces the reactivity because it produces just one reactive radical.

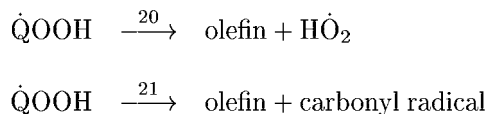
Moreover, the self reaction of hydroperoxyl radicals shows a positive sensitivity coefficient as it consumes hydroperoxyl radicals which could otherwise abstract a hydrogen atom from a stable species to ultimately produce two hydroxyl radicals from one hydroperoxyl radical, as depicted in the equation array above.



The reaction which shows the highest positive sensitivity and therefore reduces the reactivity of the system is the β -scission of the alkyl radical, reaction type 3. This reaction shows a particularly high sensitivity at 825 K, in the middle of the NTC region.

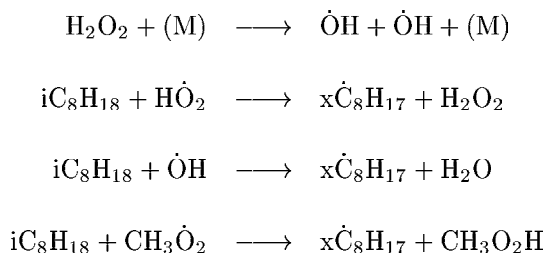
Other reactions which show a high positive sensitivity coefficient (reducing reactivity) are the decomposition reactions of the $\dot{\text{Q}}\text{OOH}$ radical, namely:





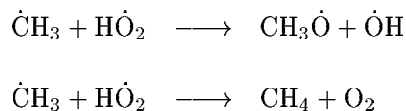
We also performed a sensitivity analysis on the flow reactor experiments of Chen *et al.* [23] at a temperature of 945 K, at 6 atm pressure and at an equivalence ratio of 0.05. We define the sensitivity coefficient as the percentage change in time taken for 20% and 60% of the fuel to be consumed. The results of this analysis are depicted in Fig. 18. A general observation is that, under these conditions, the low temperature mechanism is of minor importance. In addition, at 945 K and 6 atm, the system is in the intermediate to high temperature regime and so hydroperoxyl- and methylperoxyl radical chemistry, as described above, is important.

The reactions with the highest negative sensitivity coefficients and thus most effective in promoting the overall rate of reaction are those involving the hydroperoxyl and hydroxyl radicals. In addition, hydrogen atom abstraction by methyl-peroxy radicals is also important.



Increasing the rate of unimolecular fuel decomposition also promotes the reactivity of the system and we observe a high negative sensitivity coefficient for this type of reaction.

In addition, the $\dot{C}H_3 + \dot{H}O_2$ reaction shows a high sensitivity. The reaction producing a methoxy and a hydroxyl radical promotes reactivity while that producing methane and molecular oxygen understandably reduces the overall reactivity.



Finally, we performed a sensitivity analysis at 812 K and 900 K for the jet-stirred reactor experiments of Dagaut *et al.* [10] with 0.1% iso-octane at an equivalence ratio of 1.0, at a pressure of 10 atm, with a residence time of 1 s, at 812 K. The sensitivity coefficient is defined as the percentage change in fuel consumed

relative to the baseline case (52.1%). For consistency, an increase in fuel consumption is assigned a negative sensitivity coefficient as it corresponds with an increased overall reactivity. The results of this analysis are depicted in Fig. 19.

The experimental conditions again fall in the intermediate to high temperature oxidation regime and therefore hydroperoxyl- and methylperoxyl radical chemistry is sensitive. We see little or no sensitivity to the low temperature mechanism and a low sensitivity to unimolecular fuel decomposition.

Conclusions

A detailed chemical kinetic mechanism has been developed to simulate iso-octane oxidation over a wide range of temperature, pressure and equivalence ratio conditions. This mechanism is based on our previous modeling studies of hydrocarbon oxidation and, in particular, on our n-heptane work. The overall reactivity of iso-octane oxidation is well reproduced by the model as indicated by the good agreement between model and experiment in the shock tube experiments. In addition, experimentally quantified intermediate species profiles in flow reactors and jet-stirred reactors are well reproduced by the model, indicating that the chemical pathways leading to their formation are well understood. However, we are unhappy that, in order to reproduce the very low reactivity observed experimentally at low temperature (600–770 K), we had to decrease the rates of alkyl-peroxyl radical isomerization (reaction type 12) and peroxy-alkylhydroperoxyl radical isomerization (reaction type 23) by a factor of three relative to our n-heptane work. There must be some reason why the rates of these isomerization reactions are slower for iso-octane than for n-heptane or there may be some other pathway(s) occurring at lower temperatures that we have not accounted for.

Acknowledgements

This study was performed under the auspices of the U.S. Department of Energy by the Lawrence Livermore National Laboratory under contract No. W-7405-ENG-48. This work was supported by the US Department of Energy, Office of Transportation Technologies, Gurpreet Sing and John Garbatz program managers, and by the Office of Basic Energy Sciences, Division of Chemical Sciences, Frank Tully, program manager.

References

- [1] Zheng, J., Yang, W., Miller, D. L., and Cernansky, N. P., (2001). Publ. SAE-011025, Society of Automotive Engineers.
- [2] Kong, S-C., Marriott, C., and Reitz, R. D., (2001). Publ. SAE-011026, Society of Automotive Engineers.
- [3] Agarwal, A., Lavoie, G. A., and Easley, W., (2001). Publ. SAE-011029, Society of Automotive Engineers.
- [4] Olsson, J-O., and Johansson, B., (2001). Publ. SAE-011031, Society of Automotive Engineers.
- [5] Vermeer, D. J., Meyer, J. W., and Oppenheim, A. K., *Combust. Flame* 18, 327–336 (1972).
- [6] Fieweger, K., Blumenthal, R., and Adomeit, G., *Proc. Combust. Inst.* 25:1579–1585 (1994).
- [7] Fieweger, K., Blumenthal, R., and Adomeit, G., *Combust. Flame* 109:599–619 (1997).
- [8] Lignola, P. G., Di Maio, F. P., Marzocchiella, A., Mercogliano, R., and Reverchon, E., *Proc. Combust. Inst.*, 22:1625–1633 (1988).
- [9] D’Anna, A., Mercogliano, R., Barbella, R., and Ciajolo, A., *Combust. Sci. and Technol.* 83:217 (1992).
- [10] Dagaut, P., Reuillon, M., and Cathonnet, M., *Combust. Sci. and Technol.* 95:233–260 (1994).
- [11] Ciajolo, A., and D’Anna, A., *Combust. Flame* 112:617–622 (1998).
- [12] Griffiths, J. F., Halford-Maw, P. A., and Rose, D. J., *Combust. Flame* 95:291–306 (1993).
- [13] Cox, A., Griffiths, J. F., Mohamed, C., Curran, H., Pitz, W. J., and Westbrook, C. K., *Proc. Combust. Inst.*, 26:2685–2692 (1996).
- [14] Minetti, R., Ribaucour, M., Carlier, M., and Sochet, L. R., *Combust. Sci. and Technol.* 113–114:179–192 (1996).
- [15] Callahan, C. V., Held, T. J., Dryer, F. L., Minetti, R., Ribaucour, M., Sochet, L. R., Faravelli, T., Gaffuri, P., and Ranzi, E., *Proc. Combust. Inst.*, 26:739–746 (1996).
- [16] Minetti, R., Carlier, M., Ribaucour, M., Therssen, E., M., and Sochet, L. R., *Proc. Combust. Inst.*, 26:747–753 (1996).
- [17] Leppard, W. R., (1992). Publ. SAE-922325, Society of Automotive Engineers.

- [18] Filipe, D. J., Li, H., Miller, D. L., and Cernansky, N. P., (1992). Publ. SAE-920807, Society of Automotive Engineers.
- [19] Li, H., Prabhu, S. K., Miller, D. L., and Cernansky, N. P., (1994). Publ. SAE-942062, Society of Automotive Engineers.
- [20] Dryer, F. L., and Brezinsky, K., *Combust. Sci. and Technol.* 45:199–212 (1986).
- [21] Curran, H. J., Gaffuri, P., Pitz, W. J., Westbrook, C. K., Callahan, C., Dryer, F. L., and Held, T., *Central States/Western States/Mexican Ntl. Sections Comb. Inst.*, 1995, p. 263.
- [22] Callahan, C. V., M. S. E. Thesis, Department of Mechanical and Aerospace Engineering, Princeton University, 1995.
- [23] Chen, J.-S., Litzinger, T. A., and Curran, H. J., *Combust. Sci. and Technol.* 155:49–79 (2000).
- [24] Côme, G. M., Warth, V., Glaude, P. A., Fournet, R., Battin-LeClerc, F., and Scacchi, G. *Proc. Combust. Inst.*, 26:755–762 (1996).
- [25] Glaude, P.-A., Warth, V., Fournet, R., Battin-LeClerc, F., Côme, G. M., and Scacchi, G. *Bull. Soc. Chim. Belg.*, 106:343–348 (1997).
- [26] Ranzi, E., Faravelli, T., Gaffuri, P., Sogaro, A., D’Anna, A., and Ciajolo, A., *Combust. Flame*, 108:24–42 (1997).
- [27] Roberts, C. E., Matthews, R. D., and Leppard, W. R., (1996). Publ. SAE-962107, Society of Automotive Engineers.
- [28] Curran, H. J., Pitz, W. J., Westbrook, C. K., Callahan, C., and Dryer, F. L., *Proc. Combust. Inst.*, 27:379–387 (1998).
- [29] Davis, S. G., and Law, C. K., *Proc. Combust. Inst.*, 27:521–527 (1998).
- [30] Lund, C. M. and Chase, L., “HCT - A General Computer Program for Calculating Time-Dependent Phenomena Involving One-Dimensional Hydrodynamics, Transport, and Detailed Chemical Kinetics,” Lawrence Livermore National Laboratory report UCRL-52504, revised (1995).
- [31] Westbrook, C. K., and Dryer, F. L., *Proc. Combust. Inst.*, 18:749–767 (1981).
- [32] Westbrook, C. K., Warnatz, J., and Pitz, W. J., *Proc. Combust. Inst.*, 22:893–901 (1988).

- [33] Westbrook, C. K., Pitz, W. J., and Leppard, W. R., (1991). Publ. SAE-912314, Society of Automotive Engineers.
- [34] Chevalier, C., Pitz, W. J., Warnatz, J., Westbrook, C. K., and Melenk, H., *Proc. Combust. Inst.*, 24:92-101 (1992).
- [35] Koert, D., Pitz, W. J., Bozzelli J. W., and Cernansky, N. P., *Proc. Combust. Inst.*, 26:633-640 (1996).
- [36] Curran, H. J., Pitz, W. J., and Westbrook, C. K., Hisham, M. W. M., and Walker R. W., *Proc. Combust. Inst.*, 26:641-649 (1996).
- [37] Wang, S., Miller, D. L., Cernansky, N. P., Curran, H. J., Pitz, W. J., and Westbrook, C. K., *Combust. Flame*, 118:415-430 (1999).
- [38] Ribaucour, M., Minetti, R., Sochet, L. R., Curran, H. J., Pitz, W. J., and Westbrook, C. K., *Proc. Combust. Inst.*, 28:1671-1678 (2000).
- [39] Curran, H. J., Gaffuri, P., Pitz, W. J., Westbrook, C. K., and Leppard, W. R., (1995). Publ. SAE-952406, Society of Automotive Engineers.
- [40] Curran, H. J., Gaffuri, P., Pitz, W. J., Westbrook, C. K., and Leppard, W. R., *Proc. Combust. Inst.*, 26:2669-2677 (1996).
- [41] Curran, H. J., Gaffuri, P., Pitz, W. J., and Westbrook, C. K., *Combust. Flame*, 114:149-177 (1998).
- [42] Benson, S. W., *Thermochemical Kinetics*. John Wiley and Sons, Inc., New York, 1976.
- [43] Ritter, E. R., and Bozzelli, J. W., *Int. J. Chem. Kinet.* 23:767 (1991).
- [44] Lay, T., Bozzelli, J. W., Dean, A. M., and Ritter, E. R., *J. Phys. Chem.* 99:14514, (1995).
- [45] Lay, T., and Bozzelli, J. W., *J. Phys. Chem. A* 101:9505-9510 (1997).
- [46] Knyazev, V. D., and Slagle, I. R., *J. Phys. Chem. A* 102:1770-1778 (1998).
- [47] Curran, H. J., Fischer, S. L., and Dryer, F. L., *Intl. J. Chem. Kinet.* 32:741-759 (2000).
- [48] http://www-cms.llnl.gov/combustion/combustion_home.html
- [49] Allara, D. L., and Shaw, R., *J. Phys. Chem. Ref. Data*, Vol. 9, No. 3, pp. 523-559 (1980).
- [50] Tsang, W., *J. Phys. Chem. Ref. Data* 19:1-68 (1990).
- [51] Tsang, W., *J. Phys. Chem. Ref. Data* 17:887 (1988).

- [52] Dean, A. M., *J. Phys. Chem.* 89:4600 (1985).
- [53] Dean, A. M., Bozzelli, J. W., and Ritter, E. R., *Combust. Sci. Technol.* 80:63–85 (1991).
- [54] Bozzelli, J. W., and Pitz, W. J., *Proc. Combust. Inst.*, 25:783–791 (1994).
- [55] Edelson, D., and Allara, D. L., *Int. J. Chem. Kinet.*, 12:605 (1980).
- [56] Pollard, R. T., *Comprehensive Chemical Kinetics Vol. 17*, (C. H. Bamford and C. F. H. Tipper, Eds.), Elsevier, New York, 1977, p. 249.
- [57] Halstead, M. P., Kirsch, L. J., and Quinn, C. P., *Combust. Sci. Technol.*, 30:45–60 (1977).
- [58] Hu, H., and Keck, J. C., (1987). Publ. SAE-872110, Society of Automotive Engineers.
- [59] Cox, R. A., and Cole, J. A., *Combust. Flame*, 60:109 (1985).
- [60] Griffiths, J. F., *Prog. Energy Combust. Sci.*, 21:25–107 (1995).
- [61] Lenhardt, T. M., McDade, C. E., and Bayes, K. D., *J. Chem. Phys.* 72:304 (1980).
- [62] Dilger, H., Stolmar, M., Trogen-Piggott, P. L. W., Roduner, E., *Ber. Bunsenges Phys. Chem.* 101:956–960 (1997).
- [63] Atkinson, R., Baulch, D. L., Cox, R. A., Hampson, R. F., Jr., Kerr, J. A., Rossi, M. J., and Troe, J., *J. Phys. Chem. Ref. Data* 26:521–1011 (1997).
- [64] Xi, Z., Han, W.-J., and Bayes, K. D., *J. Phys. Chem.* 92:3450 (1988).
- [65] Keiffer, M., Miscampbell, A. J., and Pilling, M. J., *J. Chem. Soc. Farad. Trans. II.* 84:505 (1988).
- [66] Benson, S. W., *Prog. Energy Combust. Sci.* 7:125–134 (1981).
- [67] Baldwin, R. R., Hisham, M. W. M., and Walker, R. W., *J. Chem. Soc. Faraday Trans.*, I(78):1615–1627 (1982).
- [68] Hughes, K. J., Lightfoot, P. D., and Pilling, M. J., *Chem. Phys. Lett.* 191:581–586 (1992).
- [69] Robertson, P. S. H., Seakins, P. W., and Pilling, M. J., In Pilling, M. J. (Ed.), *Chemical Kinetics*. Elsevier, New York, 1997, pp. 125–234.
- [70] Lightfoot, P. D., Cox, R. A., Crowley, J. N., Destriau, M., Hayman, G. D., Jenkin, M. E., Moortgat, G. K., and Zabel, F. *Atmos. Environ. Part A*: 26:1805–1961 (1992).
- [71] Fenter, F. F., Catoire, V., Lesclaux, R., and Lightfoot, P. D., *J. Phys. Chem.* 97:3530–3538 (1993).

- [72] Maricq, M. M., and Szente, J. J. *J. Phys. Chem.* 98:2078–2082 (1994).
- [73] Tsang, W., and Hampson, R. F., *J. Phys. Chem. Ref. Data*, 15:1087 (1987).
- [74] Lightfoot, P. D., Roussel, P., Caralp, F., and Lesclaux, R., *J. Chem. Soc. Faraday Trans.*, 87(19):3213–3220 (1991).
- [75] Baulch, D. L., Cobos, C. J., Cox, R. A., Frank, P., Hayman, G., Just, Th., Kerr, J. A., Murrells, T., Pilling, M. J., Troe, J., Walker, R. W., and Warnatz, J. *J. Phys. Chem. Ref. Data* 23:847–1033 (1994).
- [76] Sahetchian, K. A., Rigny, R., De Maleissye, J. T., Batt, L., Anwar Khan, M., and Mathews, S., *Proc. Combust. Inst.*, 24:637–643 (1992).
- [77] Chen, C.-J., and Bozzelli, J. W., *J. Phys. Chem. A* 104:4997–5012 (2000).
- [78] Reinstra-Kiracofe, J. C., Allen, W. D., and Schaefer III, H. F., *J. Phys. Chem. A* 104:9823–9840 (2000).
- [79] Ray, D. J. M.; Diaz, R. R. and Waddington, D. J., *Proc. Combust. Inst.*, 14:259 (1973).
- [80] Ray, D. J. M. and Waddington, D. J., *Combust. Flame* 20:327 (1973).
- [81] Flowers, M. C. and Parker, R. M. *Intl. J. Chem. Kinet.* 3:443 (1971).
- [82] Baldwin, R. R., Dean, C. E., and Walker, R. W., *J. Chem. Soc. Farad. Trans. II.* 82:1445 (1986).
- [83] Mirokhin, Y., Mallard, W. G., Westley, F., Herron, J. T., Frizzell, D., Hampson, R., NIST Standard Reference Database 17-2Q98, Gaithersburg, MD (1998).
- [84] Cohen, N., *Intl. J. Chem. Kinet.* 14:1339 (1982).
- [85] Walker, R. W., *Proc. Combust. Inst.*, 22:883–892 (1988).
- [86] Walker, R. W. “A Critical Survey of Rate Constants for Reactions in Gas-Phase Hydrocarbon Oxidation”, in *Reaction Kinetics, Vol. 1*, (P. G. Ashmore, Ed.), The Chemical Society, Burlington House, London, 1975.
- [87] Sundaram, K. M. and Froment, G. F. *Ind. Eng. Chem. Fundam.*, 17:174–182 (1978).
- [88] Tsang, W., *J. Phys. Chem. Ref. Data* 20:221–273 (1991).
- [89] Griffiths, J. F., and Scott, S. K., *Prog. Energy Combust. Sci.* 13:161–197 (1987).

Radical	Site	Rate expression per site			Citation
		\mathcal{A}	n	\mathcal{E}_a	
$\dot{\text{H}}$	Primary (a)	7.34×10^5	2.77	8147.	† ^a
$\dot{\text{H}}$	Secondary (b)	5.74×10^5	2.49	4124.	† ^b
$\dot{\text{H}}$	Tertiary (c)	6.02×10^5	2.40	2583.	† ^c
$\dot{\text{H}}$	Primary (d)	1.88×10^5	2.75	6280.	† ^d
$\dot{\text{O}}\text{H}$	Primary (a)	2.63×10^7	1.80	278.	[84]
$\dot{\text{O}}\text{H}$	Secondary (b)	9.00×10^5	2.00	-1133.	[84]
$\dot{\text{O}}\text{H}$	Tertiary (c)	1.70×10^6	1.90	-1451.	[84]
$\dot{\text{O}}\text{H}$	Primary (d)	1.78×10^7	1.80	1431.	[84]
$\dot{\text{O}}$	Primary (a)	8.55×10^3	3.05	3123.	† ^a
$\dot{\text{O}}$	Secondary (b)	4.77×10^4	2.71	2106.	† ^b
$\dot{\text{O}}$	Tertiary (c)	6.01×10^{-10}	6.36	893.	† ^c
$\dot{\text{O}}$	Primary (d)	2.85×10^5	2.50	3645.	† ^d
$\dot{\text{C}}\text{H}_3$	Primary (a)	4.26×10^{-14}	8.06	4154.	† ^a
$\dot{\text{C}}\text{H}_3$	Secondary (b)	2.71×10^4	2.26	7287.	† ^b
$\dot{\text{C}}\text{H}_3$	Tertiary (c)	8.96×10^3	2.33	6147.	† ^c
$\dot{\text{C}}\text{H}_3$	Primary (d)	1.47×10^{-1}	3.87	6808.	† ^d
$\text{H}\dot{\text{O}}_2$	Primary (a)	2.52×10^{13}	0.0	20435.	[85]
$\text{H}\dot{\text{O}}_2$	Secondary (b)	5.60×10^{12}	0.0	17686.	[85]
$\text{H}\dot{\text{O}}_2$	Tertiary (c)	2.80×10^{12}	0.0	16013.	[85]
$\text{H}\dot{\text{O}}_2$	Primary (d)	1.68×10^{13}	0.0	20435.	[85]
$\text{CH}_3\dot{\text{O}}$	Primary (a)	4.74×10^{11}	0.0	7000.	[86]
$\text{CH}_3\dot{\text{O}}$	Secondary (b)	1.10×10^{11}	0.0	5000.	[86]
$\text{CH}_3\dot{\text{O}}$	Tertiary (c)	1.90×10^{10}	0.0	2800.	[86]
$\text{CH}_3\dot{\text{O}}$	Primary (d)	3.20×10^{11}	0.0	7000.	[86]
O_2	Primary (a)	6.30×10^{13}	0.0	50760.	† ^e
O_2	Secondary (b)	1.40×10^{13}	0.0	48210.	† ^e
O_2	Tertiary (c)	7.00×10^{12}	0.0	46060.	† ^e
O_2	Primary (d)	4.20×10^{13}	0.0	50760.	† ^e
$\dot{\text{C}}_2\text{H}_5$	Primary (a)	1.50×10^{11}	0.0	13400.	[49]
$\dot{\text{C}}_2\text{H}_5$	Secondary (b)	5.00×10^{10}	0.0	10400.	[49]
$\dot{\text{C}}_2\text{H}_5$	Tertiary (c)	1.00×10^{11}	0.0	7900.	[49]
$\dot{\text{C}}_2\text{H}_5$	Primary (d)	1.00×10^{11}	0.0	13400.	[49]
$\dot{\text{C}}_2\text{H}_3$	Primary (a)	1.50×10^{12}	0.0	18000.	[87]
$\dot{\text{C}}_2\text{H}_3$	Secondary (b)	4.00×10^{11}	0.0	16800.	[87]
$\dot{\text{C}}_2\text{H}_3$	Tertiary (c)	2.00×10^{11}	0.0	14300.	[87]
$\dot{\text{C}}_2\text{H}_3$	Primary (d)	1.00×10^{12}	0.0	18000.	[87]

Table 1: Rate constant expressions for H atom abstraction from the fuel. $\text{cm}^3\text{-mol-sec-cal}$ units.

†: This study, see text.

a: $3/4 \times$ analogous rate expression for neopentane [37].

b: NIST database [83] fit to $\text{C}_3\text{H}_8 + \dot{\text{R}} = \text{iC}_3\text{H}_7 + \text{RH}$.

c: By analogy with Tsang's [50] recommendation for $\text{iC}_4\text{H}_{10} + \dot{\text{R}} = \text{tC}_4\text{H}_9 + \text{RH}$.

d: NIST database [83] fit to $\text{C}_3\text{H}_8 + \dot{\text{R}} = \text{nC}_3\text{H}_7 + \text{RH}$.

e: As recommended by [86], $E_a \approx \Delta H$. Overall \mathcal{A} -factor of 4.0×10^{13} [86] was partitioned between 1° , 2° , and 3° .

Isomerization	Ring Size	Rate expression		
		\mathcal{A}	n	\mathcal{E}_a
aC ₈ H ₁₇ \rightleftharpoons dC ₈ H ₁₇ reverse	6	1.39×10^{11}	0.00	15400.
		4.16×10^{11}	0.00	16200.
aC ₈ H ₁₇ \rightleftharpoons cC ₈ H ₁₇ reverse	5	3.71×10^{11}	0.00	20400.
		1.86×10^{10}	0.58	26190.

Table 2: Rate constant expressions for C₈ alkyl radical isomerization reactions. cm³-mol-sec-cal units

Ring size	Site	Rate expression (per H atom)		
		\mathcal{A}	n	\mathcal{E}_a
5	Primary	1.00×10^{11}	0.0	29400.
	Secondary	1.00×10^{11}	0.0	26850.
	tertiary	1.00×10^{11}	0.0	24100.
6	Primary	1.25×10^{10}	0.0	24400.
	Secondary	1.25×10^{10}	0.0	20850.
	tertiary	1.25×10^{10}	0.0	19100.
7	Primary	1.56×10^9	0.0	22350.
	Secondary	1.56×10^9	0.0	19050.
	tertiary	1.56×10^9	0.0	17050.
8	Primary	1.95×10^8	0.0	25550.
	Secondary	1.95×10^8	0.0	22050.
	tertiary	1.95×10^8	0.0	20050.

Table 3: Rate constant expressions for R \dot{O}_2 isomerization reactions. cm³-mol-sec-cal units

Cyclic ether Ring size	Rate expression		
	\mathcal{A}	n	\mathcal{E}_a
3	6.00×10^{11}	0.0	22000.
4	7.50×10^{10}	0.0	15250.
5	9.38×10^9	0.0	7000.
6	1.17×10^9	0.0	1800.

Table 4: Rate constant expressions for cyclic ether formation from $\dot{Q}OOH$ radicals. cm³-mol-sec-cal units

Type of H atom	Radical	Site	Rate expression (per H atom)		
			\mathcal{A}	n	\mathcal{E}_a
H-C-C	$\dot{O}H$	Primary	3.83×10^7	1.53	775.
		Secondary	2.34×10^7	1.61	-35.
		Tertiary	5.73×10^{10}	0.51	64.
	$\dot{H}O_2$	Primary	3.33×10^3	2.55	15500.
		Secondary	7.40×10^3	2.60	13910.
		Tertiary	3.61×10^3	2.55	10532.
H-C-O	$\dot{O}H$	Primary	9.50×10^7	1.61	-35.
		Secondary	8.84×10^9	1.00	-149.
	$\dot{H}O_2$	Primary	3.00×10^4	2.60	13910.
		Secondary	1.08×10^4	2.55	10532.

Table 5: Rate constant expressions for H atom abstraction from cyclic ether by $\dot{O}H$ and $\dot{H}O_2$. cm³-mol-sec-cal units

Iso-octane Intermediates	Species Mole Fraction	
	Experiment	Model Prediction
carbon monoxide	2.31e-3	3.64e-3
isobutene	1.69e-3	3.52e-3
formaldehyde	1.17e-3	3.05e-3
2,2,4,4-tetramethyl-THF	1.01e-3	4.34e-4
acetone	8.18e-4	2.06e-3
2-t-butyl-3-methyloxetane	5.51e-4	1.95e-4
2-isopropyl-3,3-dimethyloxetane	4.74e-4	3.72e-4
propene	3.23e-4	4.89e-4
4,4-dimethyl-2-pentene	2.52e-4	8.09e-5
2,4,4-trimethyl-1-pentene	2.32e-4	1.48e-4
isobuteraldehyde	2.07e-4	3.53e-4
methacrolein	1.86e-4	1.64e-4
2,4-dimethyl-2-pentene	1.68e-4	1.25e-4
2,4,4-trimethyl-2-pentene	1.52e-4	2.08e-4
2,3-epoxy-2,4,4-trimethylpentane	1.43e-4	5.00e-5
isobutene oxide	1.39e-4	1.02e-4
2,2-dimethyl propanal	1.30e-4	6.02e-5

Table 6: Comparison of major intermediates formed in a CFR engine (@ 500 RPM) at 36% fuel conversion for iso-octane fuel, $\phi = 1.0$.

Figure Captions

Figure 1: Iso-octane with its four distinct sites for H-atom abstraction.

Figure 2: Simplified kinetic scheme for iso-octane oxidation.

Figure 3: 0.14% iso-octane oxidation at 1.0 atm, $\phi = 0.99$, $T = 1080$ K in a flow reactor. Experimental results (points) [20] vs model predictions for major intermediate products. Dashed line corresponds to open symbols.

Figure 4: 0.14% iso-octane oxidation at 12.5 atm, $\phi = 1.0$, $\tau = 1.8$ s in a PFR. ● O₂, ○ CO, ★ H₂O, ◇ Temperature rise. Experimental results (points) [22] vs model predictions. Dashed line corresponds to open symbols.

Figure 5: 0.09% iso-octane oxidation in a flow reactor, $\phi = 0.05$, $P = 6$ atm, $T = 945$ K. Experimental results (points) [23] vs model predictions. Dashed line corresponds to open symbols.

Figure 6: 0.09% iso-octane oxidation in a flow reactor, $\phi = 0.05$, $P = 6$ atm, $T = 945$ K. Experimental results (points) [23] vs model predictions for selected oxygenates. Dashed line corresponds to open symbols.

Figure 7: Formation of acetone *via* the Waddington mechanism.

Figure 8: Formation of 2-isopropyl-3,3-dimethyl oxetane.

Figure 9: 0.1% iso-octane oxidation at 10 atm, $\phi = 1.0$, $\tau = 1$ s in a JSR. Experimental (points) [10] and model predictions (lines). Dashed line corresponds to open symbols.

Figure 10: 0.1% iso-octane oxidation at 10 atm, $\phi = 0.5$, $\tau = 1$ s in a JSR. Experimental (points) [10] and model predictions (lines). Dashed line corresponds to open symbols. (d) The solid line with the highest peak value corresponds to xC₇H₁₄.

Figure 11: 0.1% iso-octane oxidation at 10 atm, $\phi = 1.5$, $\tau = 1$ s in a JSR. Experimental (points) [10] and model predictions (lines). Dashed line corresponds to open symbols. (d) The solid line with the highest peak value corresponds to xC₇H₁₄.

Figure 12: 2.2% iC_8H_{18} , 27.8% O_2 , 70% Ar, $P_5 = 2.1$ atm, $\phi = 0.989$. Experimental (points) [5], and model predicted ignition delay times. Dashed line corresponds to open symbols.

Figure 13: Influence of equivalence ratio for iso-octane oxidation in a shock tube at 13 bar, $\phi = 1.0$ in air. Experimental (points) [6,7] and model predictions (lines). Dashed line corresponds to open symbols.

Figure 14: Influence of equivalence ratio for iso-octane oxidation in a shock tube at 40 bar, $\phi = 1.0$ in air. Experimental (points) [6,7] and model predictions (lines). Dashed line corresponds to open symbols.

Figure 15: Influence of pressure on iso-octane oxidation in a shock tube at $\phi = 1.0$ in air. Experimental (points) [6,7] and model predictions (lines). Dashed line corresponds to open symbols.

Figure 16: ● CO and ○ O_2 formed in a CFR engine (@ 500 RPM) for iso-octane fuel, $\phi = 1.0$. Experimental results (points) [17] vs model predictions. Dashed line corresponds to open symbols.

Figure 17: Sensitivity coefficients in a shock tube [7]. Stoichiometric fuel in air, $P_5 = 40$ bar.

Figure 18: Sensitivity coefficients in a flow reactor [23] at 20% and 60% fuel conversion. 0.09% iso-octane oxidation at 6 atm, $\phi = 0.05$, $T = 945$ K.

Figure 19: Sensitivity coefficients in a JSR [10]. 0.1% iso-octane oxidation at 10 atm, $\phi = 1.0$, $\tau = 1$ s.

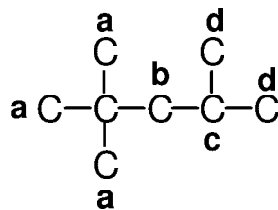


Figure 1: Iso-octane with its four distinct sites for H-atom abstraction.

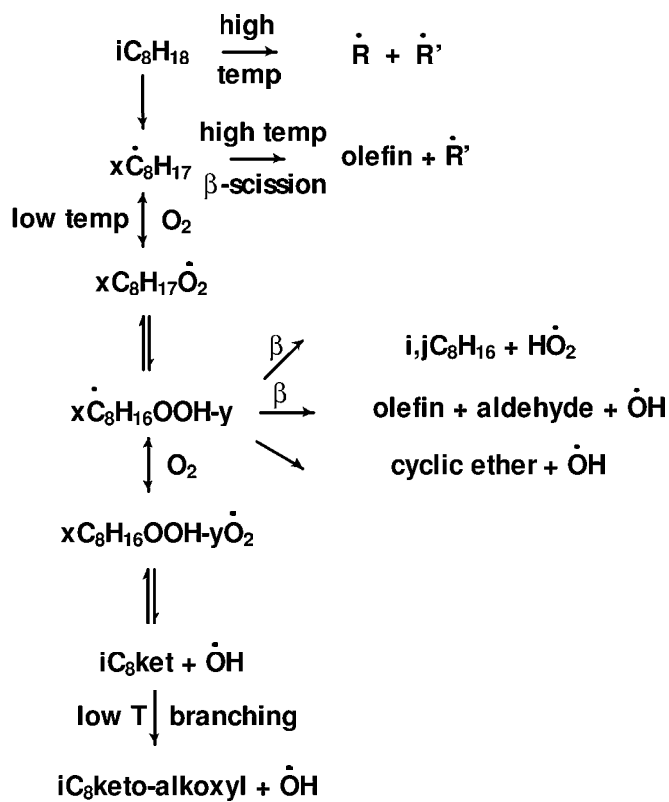


Figure 2: Simplified kinetic scheme for iso-octane oxidation.

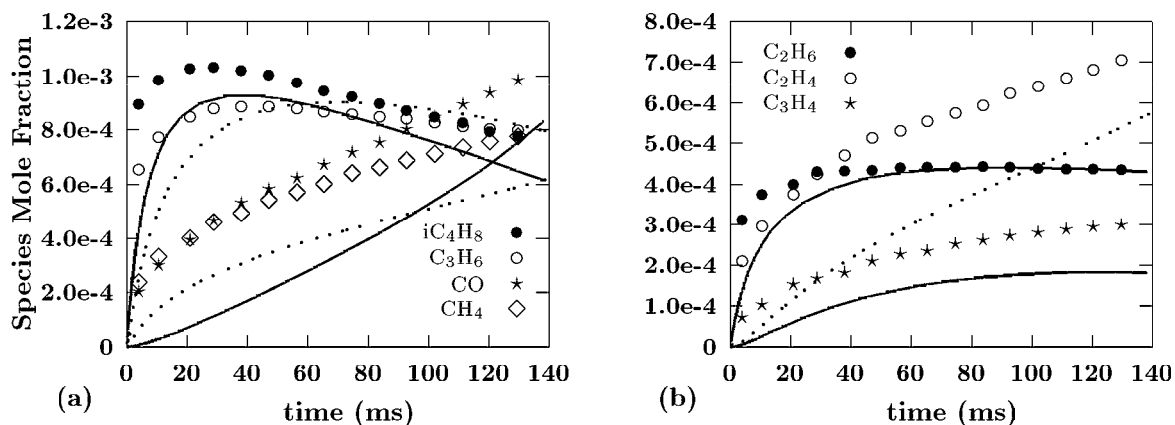


Figure 3: 0.14% iso-octane oxidation at 1.0 atm, $\phi = 0.99$, $T = 1080$ K in a flow reactor. Experimental results (points) [20] vs model predictions for major intermediate products. Dashed line corresponds to open symbols.

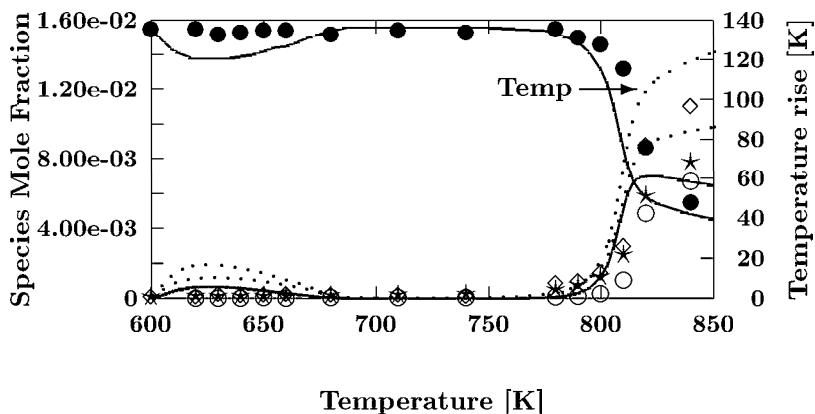
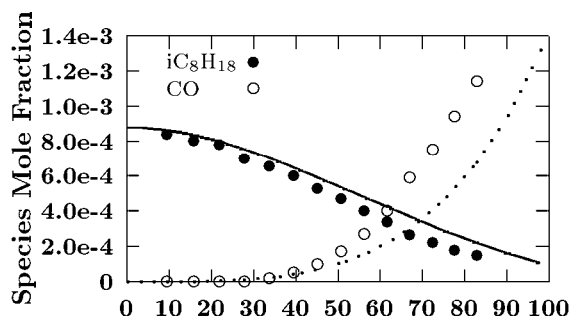
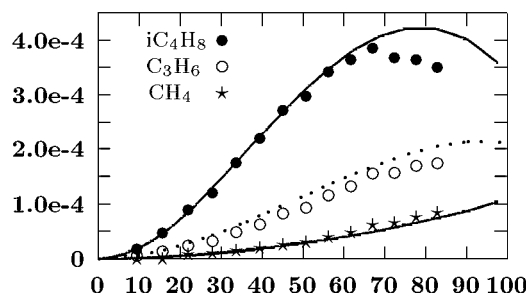


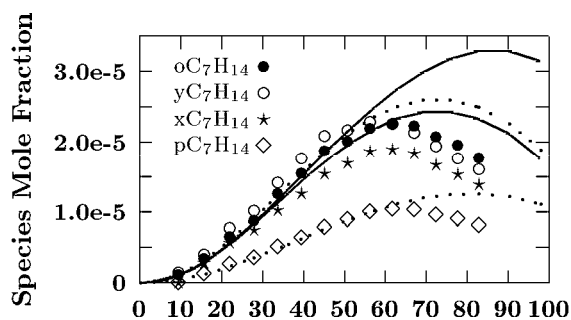
Figure 4: 0.14% iso-octane oxidation at 12.5 atm, $\phi = 1.0$, $\tau = 1.8$ s in a PFR. \bullet O_2 , \circ CO , \star H_2O , \diamond Temperature rise. Experimental results (points) [22] vs model predictions. Dashed line corresponds to open symbols.



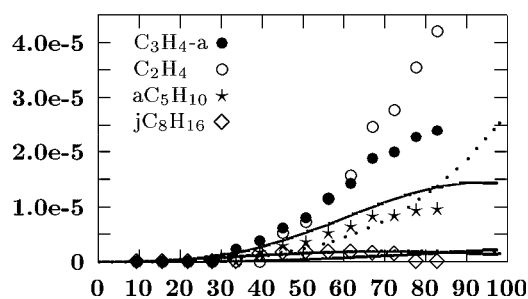
(a)



(b)

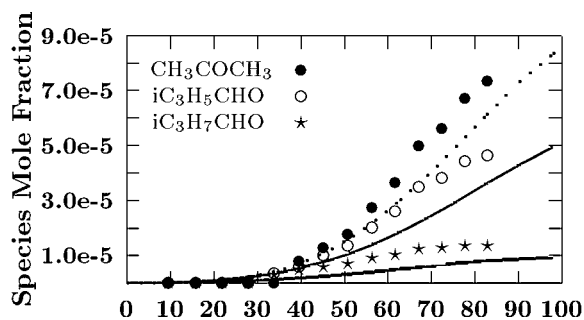


(c)

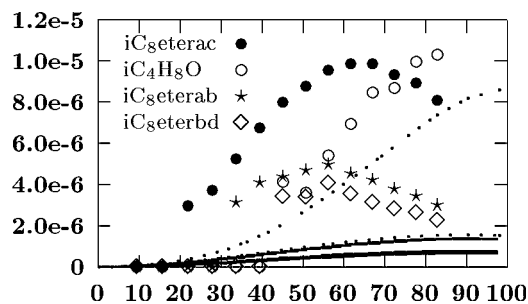


(d)

Figure 5: 0.09% iso-octane oxidation in a flow reactor, $\phi = 0.05$, $P = 6$ atm, $T = 945$ K. Experimental results (points) [23] vs model predictions. Dashed line corresponds to open symbols.



(a)



(b)

Figure 6: 0.09% iso-octane oxidation in a flow reactor, $\phi = 0.05$, $P = 6$ atm, $T = 945$ K. Experimental results (points) [23] vs model predictions for selected oxygenates. Dashed line corresponds to open symbols.

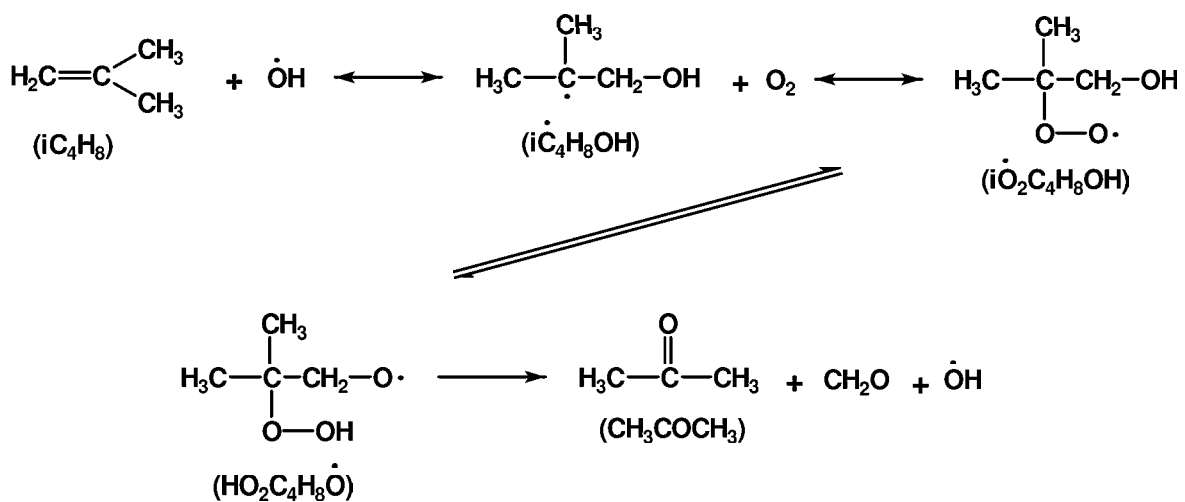


Figure 7: Formation of acetone *via* the Waddington mechanism.

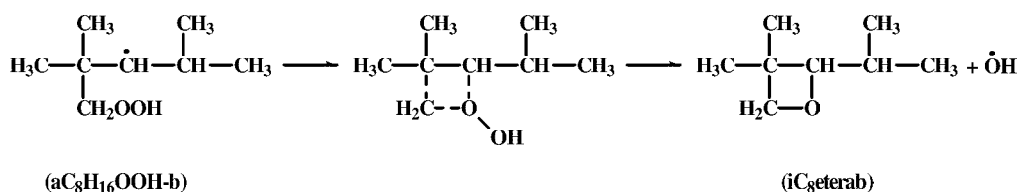
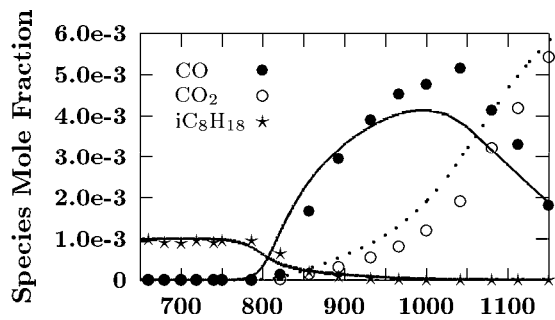
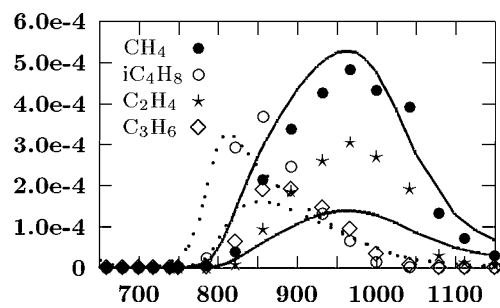


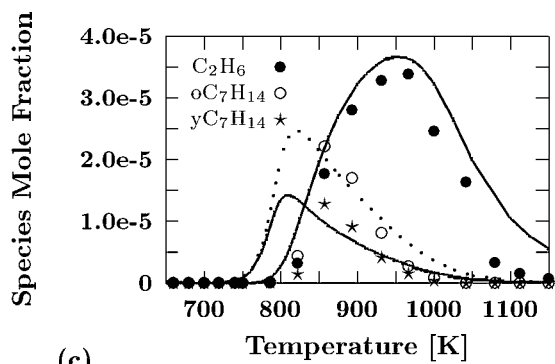
Figure 8: Formation of 2-isopropyl-3,3-dimethyl oxetane.



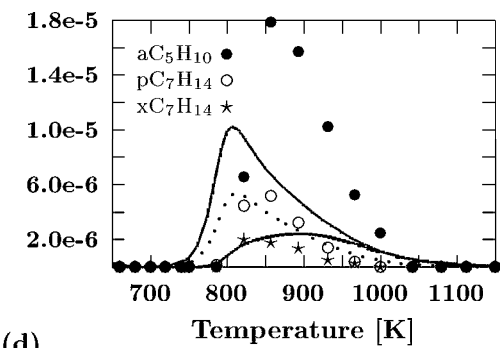
(a)



(b)

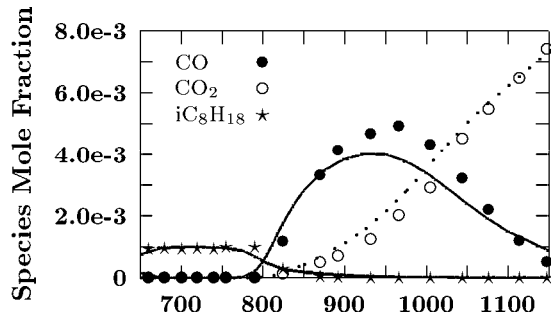


(c)

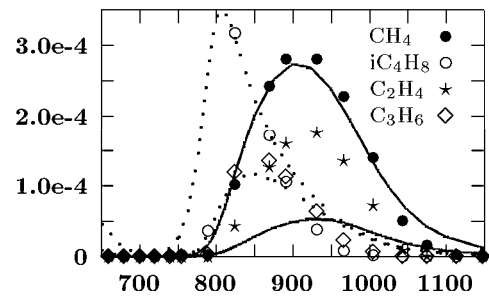


(d)

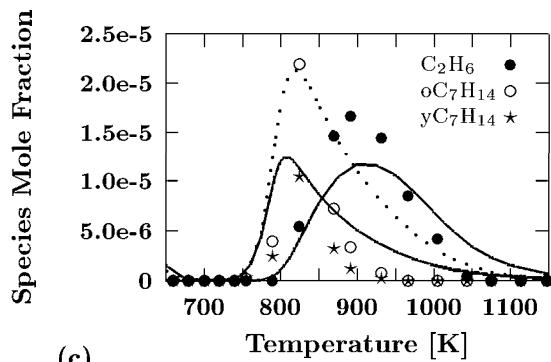
Figure 9: 0.1% iso-octane oxidation at 10 atm, $\phi = 1.0$, $\tau = 1$ s in a JSR. Experimental (points) [10] and model predictions (lines). Dashed line corresponds to open symbols.



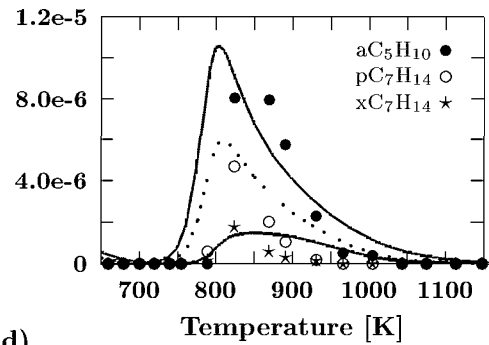
(a)



(b)



(c)



(d)

Figure 10: 0.1% iso-octane oxidation at 10 atm, $\phi = 0.5$, $\tau = 1$ s in a JSR. Experimental (points) [10] and model predictions (lines). Dashed line corresponds to open symbols. (d) The solid line with the highest peak value corresponds to $x\text{C}_7\text{H}_{14}$.

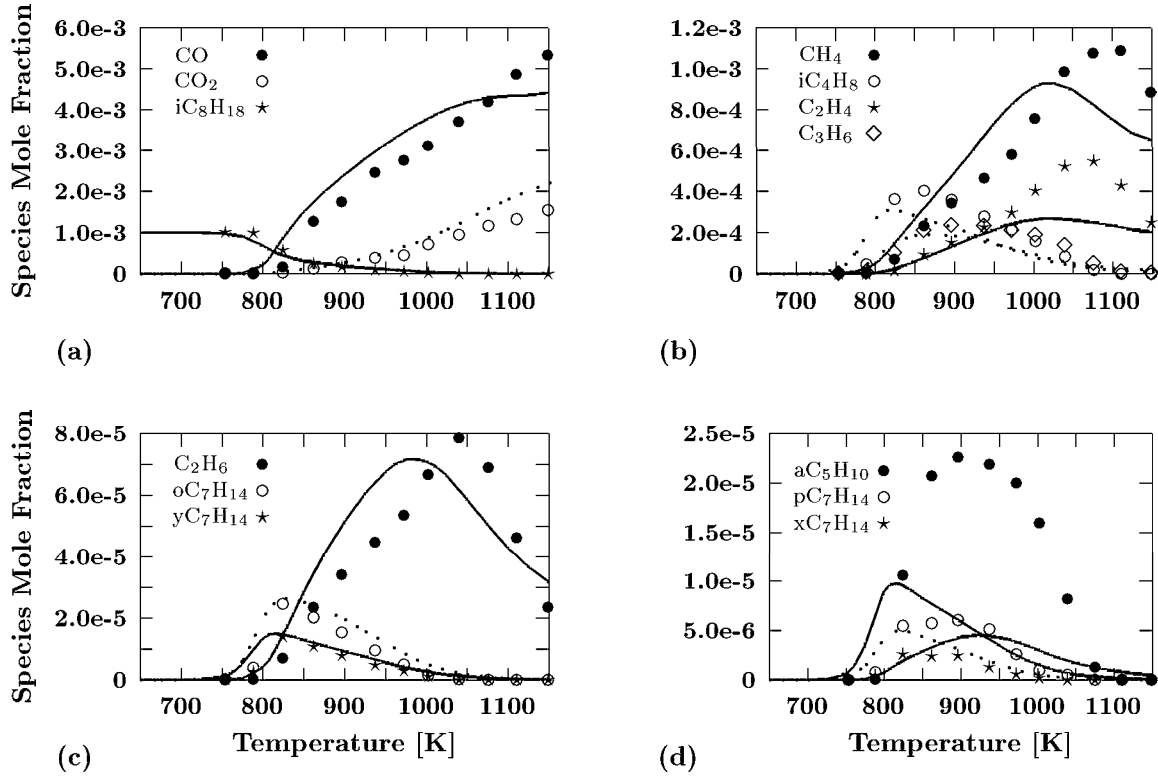


Figure 11: 0.1% iso-octane oxidation at 10 atm, $\phi = 1.5$, $\tau = 1$ s in a JSR. Experimental (points) [10] and model predictions (lines). Dashed line corresponds to open symbols. (d) The solid line with the highest peak value corresponds to xC₇H₁₄.

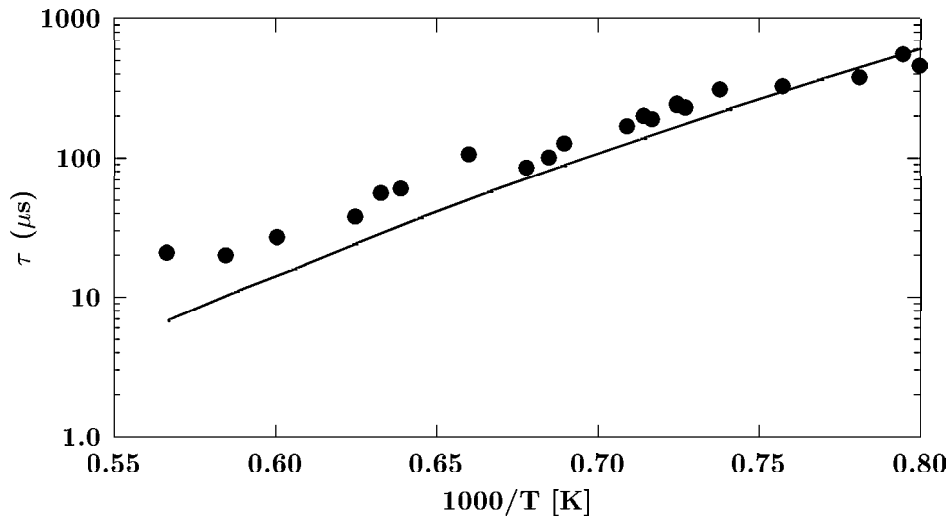


Figure 12: 2.2% iC₈H₁₈, 27.8% O₂, 70% Ar, P₅ = 2.1 atm, $\phi = 0.989$. Experimental (points) [5], and model predicted ignition delay times. Dashed line corresponds to open symbols.

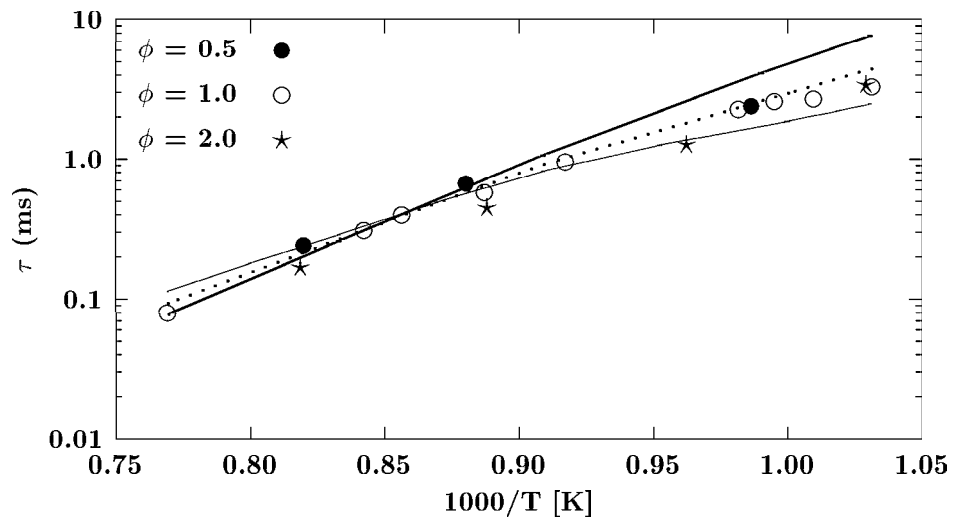


Figure 13: Influence of equivalence ratio for the oxidation of iso-octane/air mixtures in a shock tube at 13 bar. Experimental (points) [6,7] and model predictions (lines). Dashed line corresponds to open symbols.

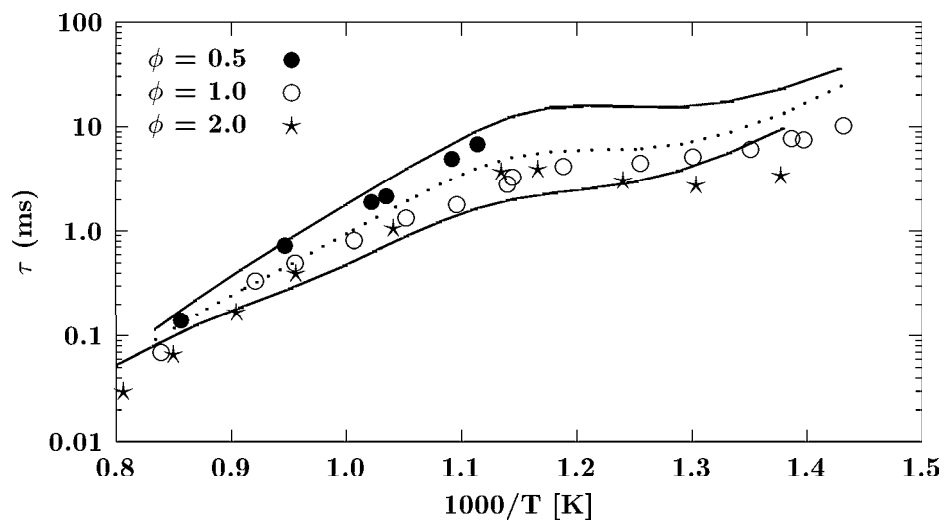


Figure 14: Influence of equivalence ratio for the oxidation of iso-octane/air mixtures in a shock tube at 40 bar. Experimental (points) [6,7] and model predictions (lines). Dashed line corresponds to open symbols.

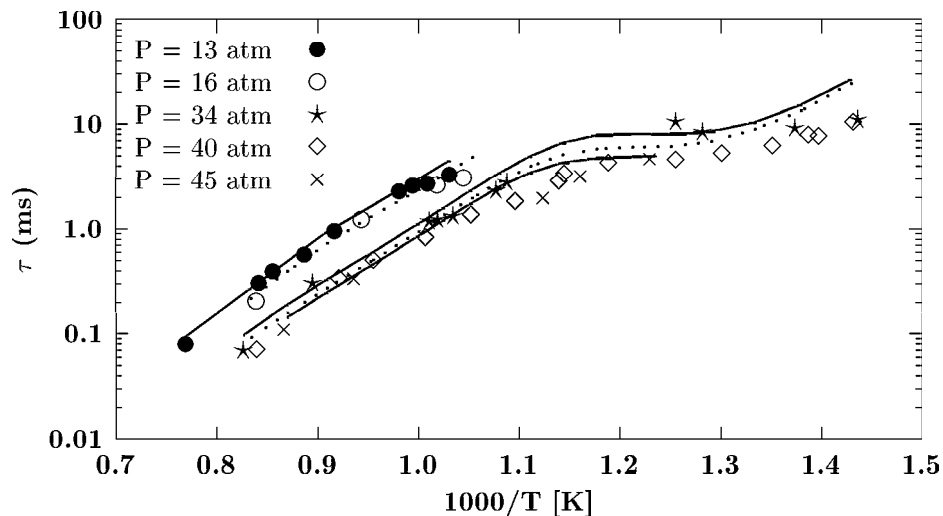


Figure 15: Influence of pressure on iso-octane oxidation in a shock tube at $\phi = 1.0$ in air. Experimental (points) [6,7] and model predictions (lines). Dashed line corresponds to open symbols.

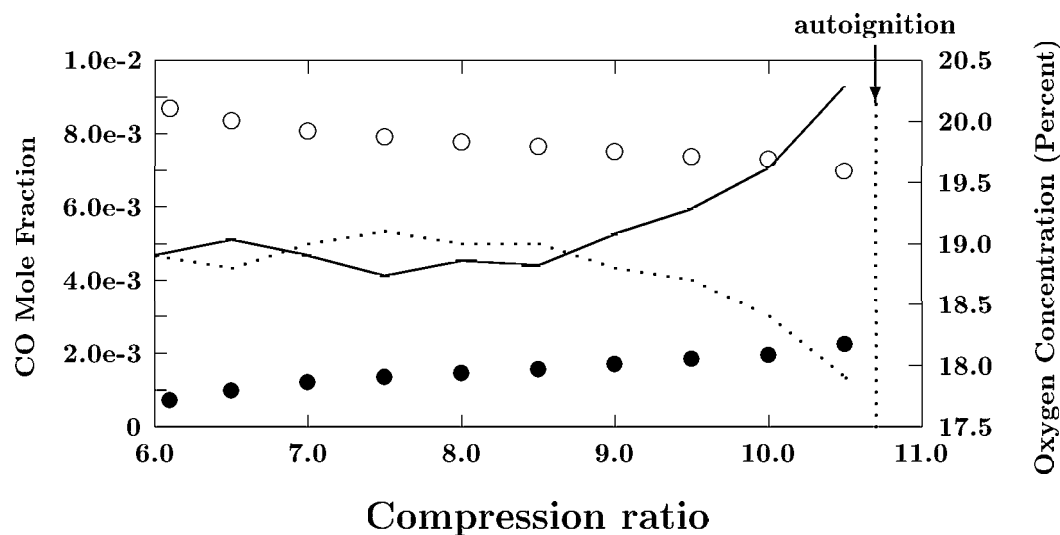


Figure 16: ● CO and ○ O₂ formed in a CFR engine (@ 500 RPM) for iso-octane fuel, $\phi = 1.0$. Experimental results (points) [17] vs model predictions. Dashed line corresponds to open symbols.

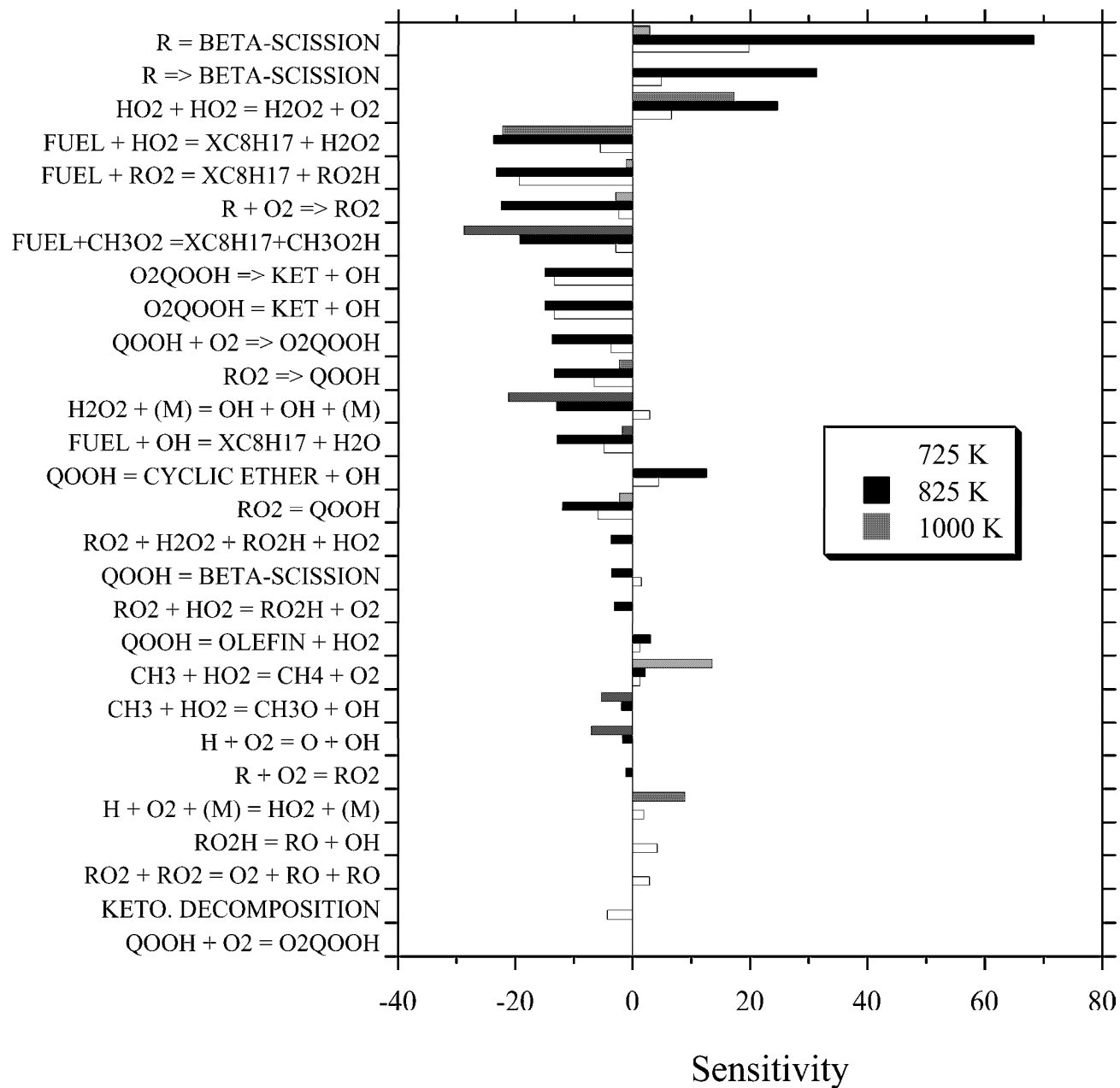


Figure 17: Sensitivity coefficients in a shock tube [7]. Stoichiometric fuel in air, $P_5 = 40$ bar.

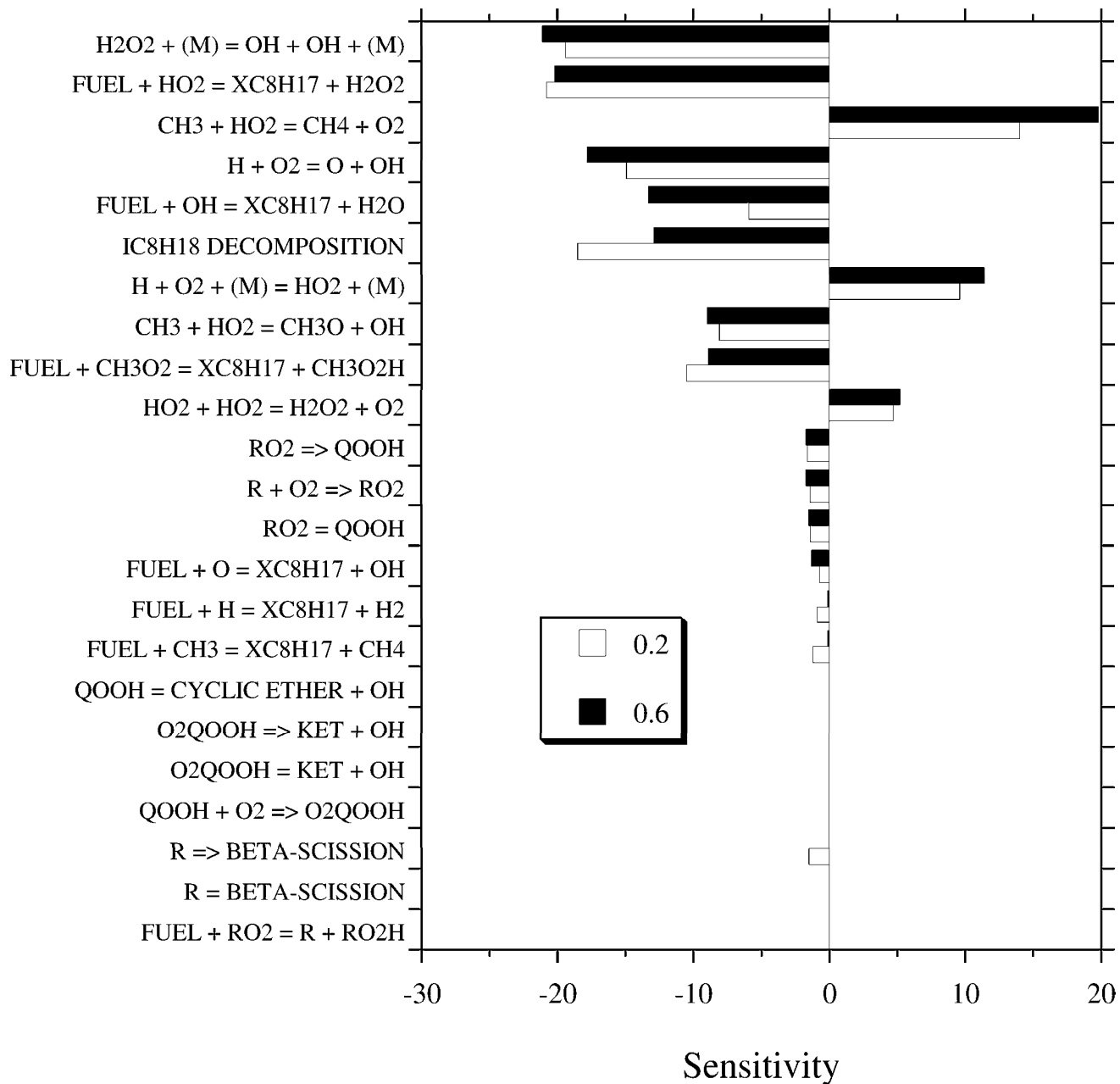


Figure 18: Sensitivity coefficients in a flow reactor [23] at 20% and 60% fuel conversion. 0.09% iso-octane oxidation at 6 atm, $\phi = 0.05$, $T = 945$ K.

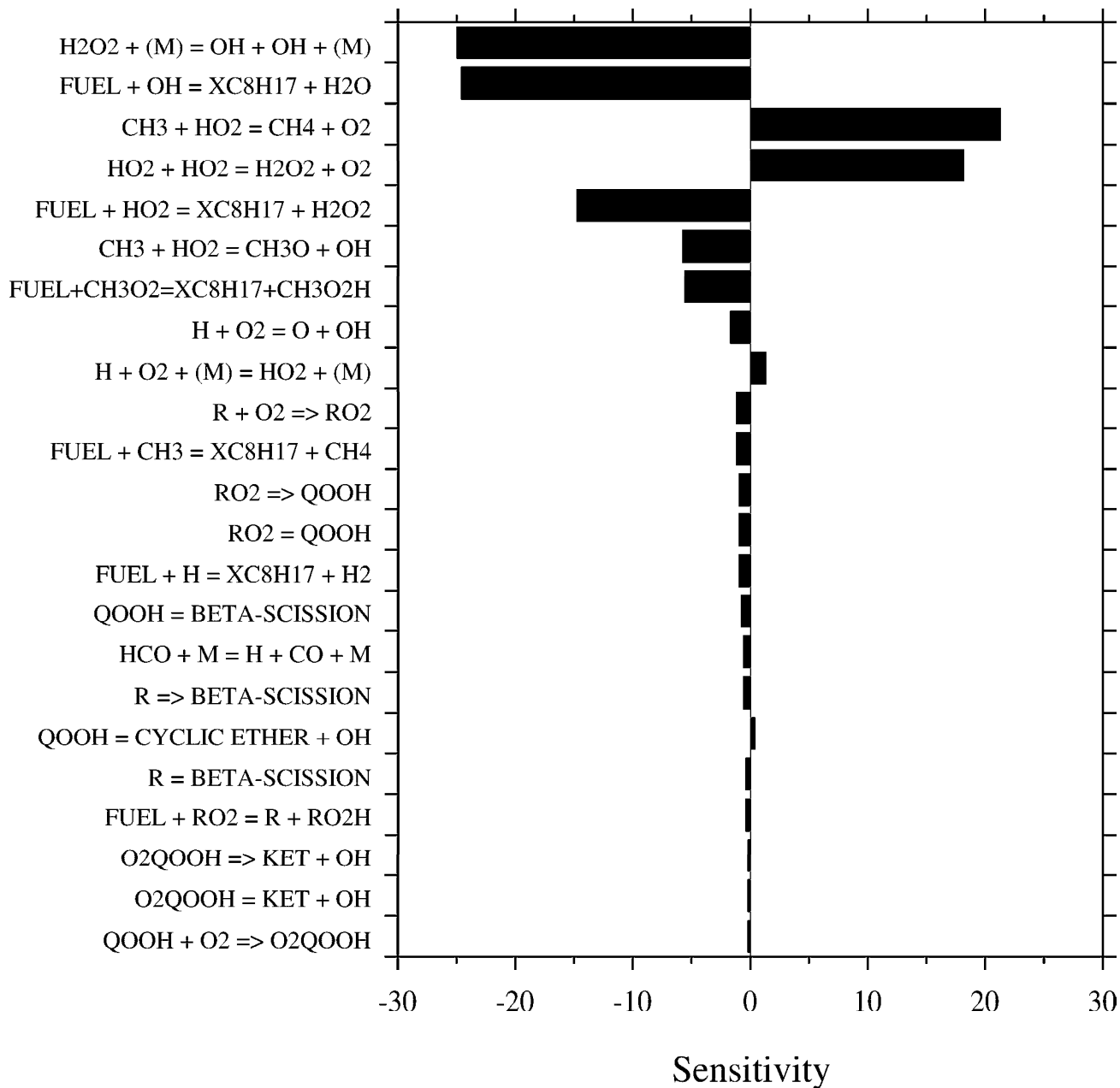


Figure 19: Sensitivity coefficients in a JSR [10]. 0.1% iso-octane oxidation at 10 atm, $\phi = 1.0$, $\tau = 1$ s.

This work was performed under the auspices of the U. S. Department of Energy by the University of California, Lawrence Livermore National Laboratory under Contract No. W-7405-Eng-48.